LITHOS 354-355 (2020) 105242

Contents lists available at ScienceDirect

LITHOS

journal homepage: www.elsevier.com/locate/lithos

Silicic volcanism triggered by increased denudation rates in the Quaternary Andean arc of central Chile between 33°50′-34°30′S

Marcia Muñoz-Gómez [a, b], Ítalo Payacán [c, d, e, *], Francisco Gutiérrez [e], Marcelo Farías [d], Reynaldo Charrier [a, d], Mireille Polvé [f]

[a] Escuela de Ciencias de La Tierra, Facultad de Ingeniería, Universidad Andres Bello, Campus República, Salvador Sanfuentes, 2357, Santiago, Chile
[b] Advanced Mining Technology Center (AMTC), Facultad de Ciencias Físicas y Matemáticas, Universidad de Chile, Av. Tupper, 2007, Santiago, Chile
[c] Escuela de Geología, Universidad Mayor, Manuel Montt 367, Providencia, Santiago, Chile
[d] Departamento de Geología, Facultad de Ciencias Físicas y Matemáticas, Universidad de Chile, Casilla, 13518, Correo 21, Santiago, Chile
[e] GeoExpedition, Las Palomas 25, Pirque, Santiago, Chile
[f] GET, Université de Toulouse, CNRS, IRD, OMP, Av. Edouard Belin, 31400, Toulouse, France

ARTICLE INFO

Article history:
Received 19 May 2019
Received in revised form
10 October 2019
Accepted 11 October 2019
Available online 24 October 2019

Keywords:
Andes
Quaternary arc
Silicic volcanism
Denudation
Numerical models

ABSTRACT

In central Chile (33°50′-34°30′S), the Quaternary arc records a distinctive episode of silicic volcanism (SiO_2 >70 wt%) that occurred during latest Pleistocene (0.1−1 Ma). This episode is recorded in several eroded and inactive arc centers distributed mostly along the highest summits of the Andes in the same region covered by the modern arc centers. We report new data including field observations, petrography, whole rock chemical and Sr-Nd isotopic analyses, mineral chemistry and geochronology for the Quaternary Andean arc in the region with emphasis in the latest Pleistocene units (0.1−1 Ma). The silicic episode that the latter units represent constitutes a singularity in the common compositions that characterize in the long term this arc segment, as it is preceded and followed by basaltic andesite-andesite-dacite suite compositions. In addition, it occurs coevally with a period of increased denudation resulting from the major uplift event of the Andean orogen in the area. Geologic field markers, supported by thermobarometric estimations, indicate conservative estimates of denudation of ~1.5 km during this period in the area which in turn accounts for a significant pressure decrease at upper crustal levels that must have affected the shallow reservoirs that fed the arc volcanoes. For evaluating this, thermodynamic numerical simulations have been run at different pressure conditions in order to describe for such magmatic systems the evolution in terms of major element composition, degree of crystallinity and volatile content with the temperature decrease. Overall, results show that the compositional spectra defined by this arc segment can be reproduced by low pressure (<0.75 kbar) crystallization of its most basic members by batch and/or fractional processes, the latter being indispensable to reproduce the most evolved compositions. Results also show that a sudden pressure decrease creates a unique set of conditions that constructively operate for prompting the rapid generation and extraction of silicic melts, among the main factors it is highlighted the sudden devolatilization and enhanced crystal-melt segregation which is expected to lead to the rapid creation of a volatile saturated silicic cap in the magma reservoirs. This in turn can account for a compositional change of the volcanoes that tap them, as is seen in the evolution of the Quaternary Andean arc in the study area. The transitory nature of such silicic volcanic episode, characterized by a return to the basaltic andesite-andesite-dacite suite compositions, follows from the transience of the increased denudation event and marks the reaching of a new steady state for the tectono-magmatic system.

1. Introduction

Regional scale episodes of silicic volcanism (SiO_2 > 70 wt%) are a common feature that occurs sporadically throughout the evolution of cordilleran arc orogenic systems. In these settings, where the dynamic interplay between magmatism and tectonics is the rule,

* Corresponding author. Departamento de Geología, Facultad de Ciencias Físicas y Matemáticas, Universidad de Chile, Casilla, 13518, Correo 21, Santiago, Chile.
E-mail addresses: marcia.munoz@unab.cl (M. Muñoz-Gómez), ipayacan@gmail.com (Í. Payacán), francisco@geoexpedition.cl (F. Gutiérrez), mafarias@ing.uchile.cl (M. Farías), rcharrier@unab.cl (R. Charrier), mireillepolve@free.fr (M. Polvé).

https://doi.org/10.1016/j.lithos.2019.105242
0024-4937/

such transient state of the arc system is thought to be variably related to particular stages and/or processes of orogenic evolution. Among the main ones, they include partial melting of tectonically thickened crust (e.g., Kay et al., 1999; Ducea and Barton, 2007) and high heat flow supply events after slab steepening and/or lithospheric delamination processes (e.g. Kay and Kay, 1993; Schnurr et al., 2007; DeCelles et al., 2009). However suitable in each case, such genetic models have not considered the role of denudation, which constitutes the geological response to the uplifting that follows from them. Unroofing of several hundred to thousand meters in relatively short time scales (<3 m.y.) is common in orogenic systems and entails a significant impact in the lithostatic pressure conditions in the upper crust. Regardless of the multi-component and multi-stage character of magmatic processes, the ultimate source of most volcanism are the shallow (<7 km) crustal magma chambers that feed the arc volcanoes and they are unlikely to remain passive to these changes.

In this contribution we explore the role of increased denudation, in response to uplifting of the Andes, over the evolution of the coeval Quaternary magmatic arc in Central Chile between 33°50 and 34°30′S (Fig. 1). This area follows a rather simple orogenic history, characterized by crustal thickening and associated uplifting and denudation, devoid of the particular stages and/or processes mentioned above (e.g., Charrier et al., 2002; Giambiagi and Ramos, 2002; Nyström et al., 2003; Kay et al., 2005; Farías et al., 2008, 2010). We report here new data from a regional scale survey in the area which includes field observations, petrography, whole rock chemical and Sr-Nd isotopic analyses, mineral chemistry and geochronology. This is used, along with previously published information, to characterize the geologic evolution of the region and we use numerical models to assess the impact of increased denudation over magmatic processes in the shallow arc reservoirs.

2. Geological background

2.1. Tectonic setting

The modern Andes correspond to a cordilleran arc orogenic

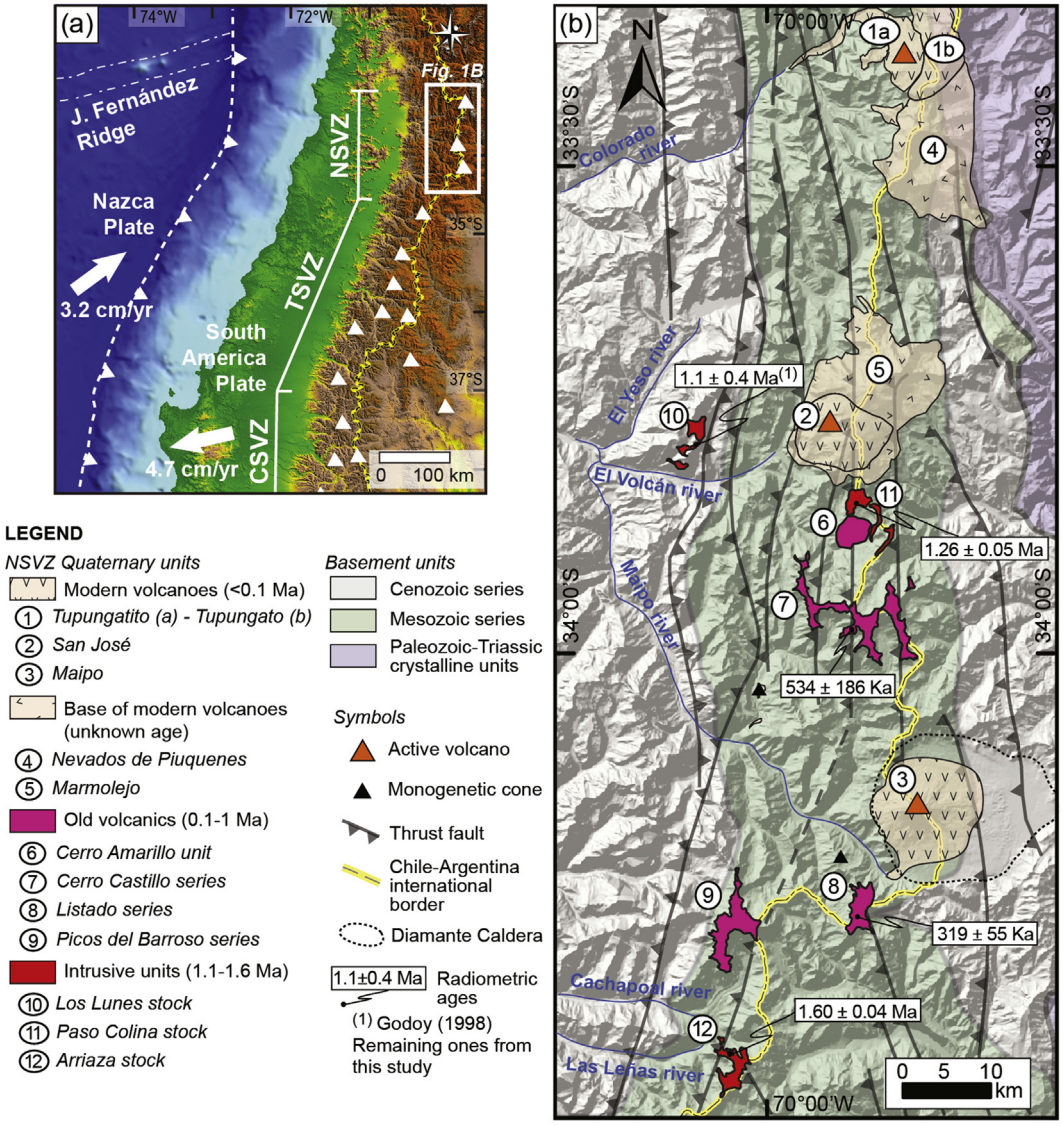

Fig. 1. Tectonic context and main geologic features of the study area. (a) Digital Elevation Model (DEM) showing the tectonic setting of the Southern Central Andes. The arrows indicate the absolute plate motion of the Nazca and South America plates. White triangles correspond to main volcanoes of the Southern Volcanic Zone (SVZ) grouped according to the Northern (NSVZ; 33–34.5°S), Transitional (TSVZ; 34.5–37°S) and Central (CSVZ; 37–42°S) segments. (b) Geologic map showing the main features relevant to this work of the study area. Modified from Thiele (1980), Charrier (1981) and this work.

system distributed along the western margin of South America. They are a first order result of the plate tectonic convergence configuration, where the Nazca oceanic plate is eastwardly subducting below the South American continental plate (Fig. 1a). Nowadays, the convergence is nearly orthogonal, with a NE-SW obliquity ~22–30°, at a rate of 7–9 cm/y (DeMets et al., 1990), and for the central Chile region (~33°–34°30′S) it shows a normal subduction dip angle of ~25–27° (Cahill and Isacks, 1992; Pardo et al., 2002, Fig. 1a). Overall, the Andean orogen corresponds to an asymmetric doubly-vergent deformed and uplifted area involving Cenozoic and Mesozoic volcanic and sedimentary sequences in Chile and Argentina, and Late Paleozoic to Triassic crystalline basement in Argentina (Fig. 1b). Near the international border the orogen hosts the currently active volcanic arc represented in a series of stratovolcanoes running mostly parallel to the main strike of the mountain belt (Fig. 1). In central Chile, between ~33° and 34°30′S, this volcanism composes the so called Northern Southern Volcanic Zone (NSVZ; Fig. 1), the northernmost segment of the ~1.400 km long Southern Volcanic Zone (SVZ) of the Andes (~33°-46°S; e.g. Stern et al., 2007).

2.2. The Quaternary Andean arc in central Chile

The currently active NSVZ distributes in a nearly north-south chain, located ~290 km to the east of the trench, along the highest Andean summits in the Chile-Argentina drainage divide (Fig. 1). It reaches between 6.500 and 5.200 m in heights that diminish steadily from north to south in accordance to crustal thicknesses that diminish from ~60 to 50 km (Tassara et al., 2006). The modern arc in this area represents the Holocene configuration of the protracted and continued Cenozoic arc magmatic activity that developed in the margin throughout the construction of the modern orogen. Initially located further west, such activity progressively migrated ~80 km eastwards since Oligocene until reaching its current location (e.g., Stern, 1989; Stern and Skewes, 1995; Kay et al., 2005). Although the modern arc did not fully establish in this position until Pleistocene, several intrusive units exposed in the area record magmatic activity since at least 8 Ma (Muñoz et al., 2013). In the region, the exposed basement that hosts such igneous activity corresponds to intensively deformed and faulted Mesozoic sedimentary sequences (Fig. 1b). Overall, all Cenozoic magmatism from central Chile shows the typical compositional features of arc-related magmas, with a variable involvement of crustal components, and has resulted from the continuous plate convergence throughout this period (e.g., Hildreth and Moorbath, 1988; Stern, 1991; Stern and Skewes, 1995; Nyström et al., 2003; Kay et al., 2005; Muñoz et al., 2013; Holm et al., 2014).

The youngest activity of the NSVZ is represented by several well preserved and mostly active stratocones, and scarce minor centers, of latest Pleistocene to Holocene ages. From north to south, the main centers correspond to: Tupungato-Tupungatito (6.570 m), San José (5.856 m) and Maipo (5.290 m) volcanoes (Fig. 1b). These units are characterized by a predominance of andesites and subordinated dacites and basaltic andesites reaching up to 67% of SiO_2 contents (all major oxides expressed as wt.%). A series of older upper Pleistocene volcanic deposits, which are more intensively affected by glacial erosion, represent the volcanic episode that immediately predates the current volcanism of the NSVZ. Also along the high summits of the Andes, they distribute as isolated units or constitute locally the base of the younger volcanic edifices and have been attributed to the remnants of extinct volcanoes (Fig. 1b; Charrier, 1981; Schneider et al., 1988; Harrington, 1989; Stern et al., 2007). These remain poorly studied, due to both its inactive nature and the difficulty of performing filed studies in the high Andes geography, and from north to south they correspond to: Nevado de Piuquenes (6.019 m), Cerro Marmolejo (6.108 m), Cerro Amarillo (4.162 m), Cerro Castillo (5.485 m), the Diamante Caldera (~3.500 m), Cerro Listado (4.250 m), and Picos del Barroso (5.000 m; Fig. 1b; Schneider et al., 1988; Stern et al., 2007). In our study area, between 33°50′ and 34°30′S, early works highlighted the distinctive acid nature of the magmatism related to the latter units. These correspond to large rhyolitic to dacitic eruptive centers characterized by a predominance of thick lava flows, with minor associated dome building and domo complexes, with a few reported SiO_2 contents between 71 and 75% (Charrier, 1981; Schneider et al., 1988; Harrington, 1989; Godoy and Hildreth, 2001). We address such units in detail in the following, except for the Picos del Barroso unit which was unreachable in the field work performed. The northernmost region of the NSVZ segment, which hosts the Nevado de Piuquenes and Cerro Marmolejo units (Fig. 1b), fall outside of our study area and its characteristics remain largely unknown except for scarce isolated reports (e.g. Hildreth and Moorbath, 1988; González-Ferrán, 1995).

3. Methods

This work is based in two consecutive lines of development. First, results from field work, petrography and analytical data are presented and discussed along with the scarce bibliographic information available. This is done in order to establish and characterize the occurrence of a silicic volcanic episode during the Late Pleistocene evolution of the NSVZ and, in addition, to show its contemporaneity to an increased erosion event in the area. Analytical data includes Ar-Ar age determinations (n = 4; n: number of samples; Supplementary Material Item 1), whole rock chemical and Sr-Nd composition (n = 8; Table 1), and mineral chemistry (n = 4, 163 analyses; Supplementary Material Item 2) and the analytical procedures are included in the Supplementary Material (Item 3). Second, we present numerical models to assess our hypothesis, that is to evaluate the effects of a sudden pressure decrease over the shallow reservoirs feeding the arc volcanoes. This is done using the Rhyolite MELTS thermodynamic software (Gualda et al., 2012; Ghiorso and Gualda, 2015) and further details on this are given in the following in the corresponding section.

4. Field and analytical data: results and discussions

4.1. Previous stages of the modern andean arc between 33°50′-34°30′S

We present in the following a general characterization of the main arc units dispersed in the study area which predate the currently active volcanism of the NSVZ, the latter which has developed mostly during Holocene (<0.01 Ma). According to their characteristics, these units can be divided in two groups: (i) the inactive and eroded centers, developed broadly between 0.1 and 1 Ma (latest Pleistocene), and (ii) earlier units which are represented exclusively in the area by intrusive rocks with ages between ~1–1.6 Ma (late Pleistocene; Fig. 1b).

4.1.1. The latest pleistocene stage (~0.1–1 Ma): inactive and eroded arc centers

4.1.1.1. Cerro Castillo and Cerro Listado. These latest Pleistocene volcanic series correspond to two different units (Fig. 1b) but they are described together as they show numerous similarities. Characteristically, they are exposed in the field as a thick package of a lava flows series, of tens to few hundred meters thick, exposed along the highest summits of the drainage divide where they constitute a discontinuous volcanic plane cut by the abrupt topography (Fig. 2a, b, c). Such series distribute mainly with a subhorizontal disposition, showing local variations in the dip angles, and discordantly overlays the Mesozoic deformed basement

Table 1
Whole rock geochemical and Sr-Nd isotope analyses.

Sample	MM13	MM14	MM5	MM6	MM4	MLL8	MLL9	RB11
Rock type	lava	lava	lava	lava	intrusive	intrusive	intrusive	intrusive
Classif.	Cpx rhyolite	Bt rhyolite	Opx rhyolite	Opx rhyolite	Amph diorite	Cpx diorite	Cpx diorite	Bt andesitic dike
Unit	Cerro Listado series	Cerro Listado series	Cerro Castillo series	Cerro Castillo series	Paso Colina stock	Arriaza stock	Arriaza stock	Los Lunes stock
Age (Ma)	0.319	0.319	0.534	0.534	1.26	1.60	1.60	1.10
Latitude	34°15′S	34°15′S	33°58′S	33°58′S	33°51′S	34°24′S	35°24′S	33°46′S
Longitude	69°54′W	69°54′W	69°54′W	69°54′W	69°54′W	70°04′W	71°04′W	70°06′W
Major Elements (wt.%)								
SiO_2	69.10	71.50	70.58	69.96	60.20	53.60	54.50	59.00
TiO_2	0.23	0.22	0.40	0.38	0.67	0.98	1.10	0.80
Al_2O_3	14.30	15.20	14.63	15.33	17.90	18.80	17.70	17.50
$Fe_2O_3^{total}$	–	–	2.72	2.87	–	–	–	–
Fe_2O_3	0.94	0.49	–	–	3.14	1.81	1.57	3.38
FeO	1.08	0.36	–	–	1.92	5.32	5.20	1.56
MnO	0.06	0.02	0.06	0.07	0.08	0.11	0.10	0.08
MgO	0.28	0.11	0.57	0.49	2.41	4.70	4.65	2.48
CaO	1.38	1.37	2.77	2.98	4.60	7.82	7.61	5.28
Na_2O	4.65	4.86	4.14	4.41	4.22	4.32	4.45	4.61
K_2O	4.18	3.93	3.03	2.74	2.27	1.48	1.52	2.04
P_2O_5	0.07	0.08	0.19	0.22	0.26	0.25	0.28	0.27
LOI	3.35	1.46	0.58	0.40	2.30	0.59	0.86	2.86
Total	99.62	99.60	99.67	99.85	99.97	99.78	99.54	99.86
Trace Elements (ppm)								
V	17.12	17.24	37.52	38.75	88.85	177.21	176.56	116.73
Cr	2.55	2.57	3.19	3.32	30.22	63.73	68.92	22.38
Co	bdl	bdl	3.78	3.60	11.92	25.22	23.53	11.95
Ni	8.89	7.25	9.59	11.14	20.51	36.27	43.52	18.70
Zn	79.16	49.29	66.35	91.18	147.52	113.48	122.08	150.99
Ga	119.03	115.50	95.06	92.05	83.24	64.30	67.28	78.14
Ge	2.43	1.55	2.20	1.89	2.85	3.24	3.36	2.85
As	7.36	bdl	bdl	bdl	bdl	5.83	bdl	bdl
Rb	116.58	112.19	71.59	71.37	58.42	38.49	37.83	47.73
Sr	142.17	141.07	414.11	398.11	445.19	562.14	579.09	588.52
Y	25.07	23.10	12.28	11.96	12.30	13.59	13.75	8.71
Zr	192.27	144.12	199.54	171.76	150.90	114.28	142.81	115.67
Nb	13.17	10.67	12.67	11.24	7.99	4.70	5.49	5.95
Mo	3.30	2.49	2.43	3.33	2.63	bdl	2.81	bdl
Sn	3.48	1.68	1.51	2.35	1.91	1.75	2.19	1.47
Sb	0.99	bdl	0.98	1.11	0.70	0.86	1.12	1.80
Cs	4.20	2.18	2.12	1.02	1.72	1.72	1.68	1.08
Ba	741.02	755.64	604.41	579.79	479.21	340.79	360.47	427.07
La	41.91	41.14	34.41	32.60	26.54	19.37	22.45	22.69
Ce	77.75	75.30	59.00	57.10	45.97	34.96	40.14	39.28
Pr	8.98	8.90	6.83	6.58	5.42	4.57	5.33	4.84
Nd	34.25	32.77	24.12	23.54	21.27	18.95	21.70	20.17
Sm	6.67	6.42	4.33	4.18	4.10	4.36	4.59	4.14
Eu	1.09	1.02	1.16	1.11	1.15	1.21	1.26	1.20
Gd	6.14	5.94	3.67	3.56	3.82	3.80	4.40	3.78
Tb	0.91	0.84	0.50	0.46	0.49	0.52	0.54	0.42
Dy	5.06	5.05	2.45	2.43	2.68	2.81	2.99	2.10
Ho	1.01	0.95	0.46	0.46	0.49	0.57	0.53	0.31
Er	3.14	2.98	1.48	1.48	1.36	1.64	1.57	bdl
Tm	0.49	0.42	0.20	0.18	0.19	0.22	0.20	0.11
Yb	3.15	2.80	1.44	1.42	1.21	1.38	1.25	0.65
Lu	0.49	0.41	0.24	0.23	0.18	0.21	0.19	0.10
Hf	6.44	4.50	5.38	4.45	4.56	3.40	4.10	3.38
Ta	1.22	0.88	0.97	0.80	0.65	0.53	0.54	0.61
W	1.23	1.08	bdl	bdl	1.08	bdl	bdl	bdl
Tl	0.62	0.56	0.36	0.33	0.28	0.12	0.18	0.27
Pb	23.87	24.97	27.11	18.38	19.18	11.03	18.27	33.88
Th	13.12	12.19	8.81	8.06	6.46	4.13	4.55	5.28
U	3.31	3.20	2.42	2.22	1.83	1.07	1.16	1.68
Sr-Nd isotopes								
$^{87}Sr/^{86}Sr$	0.70565	0.70567	0.70471	0.70470	0.70496	0.70496	0.70498	0.70447
2σ	0.00001	0.00001	0.00001	0.00001	0.00002	0.00001	0.00001	0.00002
$^{87}Sr/^{86}Sr_I$	0.70564	0.70566	0.70470	0.70470	0.70495	0.70495	0.70497	0.70447
$^{143}Nd/^{144}Nd$	0.512528	–	0.512594	0.512587	0.512629	0.512584	0.512580	0.512700
2σ	0.000008	–	0.000010	0.000014	0.000008	0.000009	0.000015	0.000007
$^{143}Nd/^{144}Nd(t)$	0.512528	–	0.512594	0.512587	0.512628	0.512583	0.512579	0.512699
εNd	−2.1	–	−0.9	−1.0	−0.2	−1.1	−1.1	1.2
$εNd_I$	−2.1	–	−0.9	−1.0	−0.2	−1.0	−1.1	1.2
2σ	0.2	–	0.2	0.3	0.2	0.2	0.3	0.1

Notes: For isotopic ratios calculations a ^{147}Sm decay constant of 6.54×10^{-12} and a ^{87}Rb decay constant of 1.42×10^{-11} were used. For $\varepsilon_{Nd}(t)$ values the chondritic ratios of $^{143}Nd/^{144}Nd = 0.512638$ and $^{147}Sm/^{144}Nd = 0.1968$ (Jacobsen and Wasserburg, 1980) were used along with the corresponding formation ages. Acronyms. Ol: olivine; Cpx: clinopyroxene; Bt: biotite; Opx: orthopyroxene; Amph: amphibole; bdl: below detection limits.

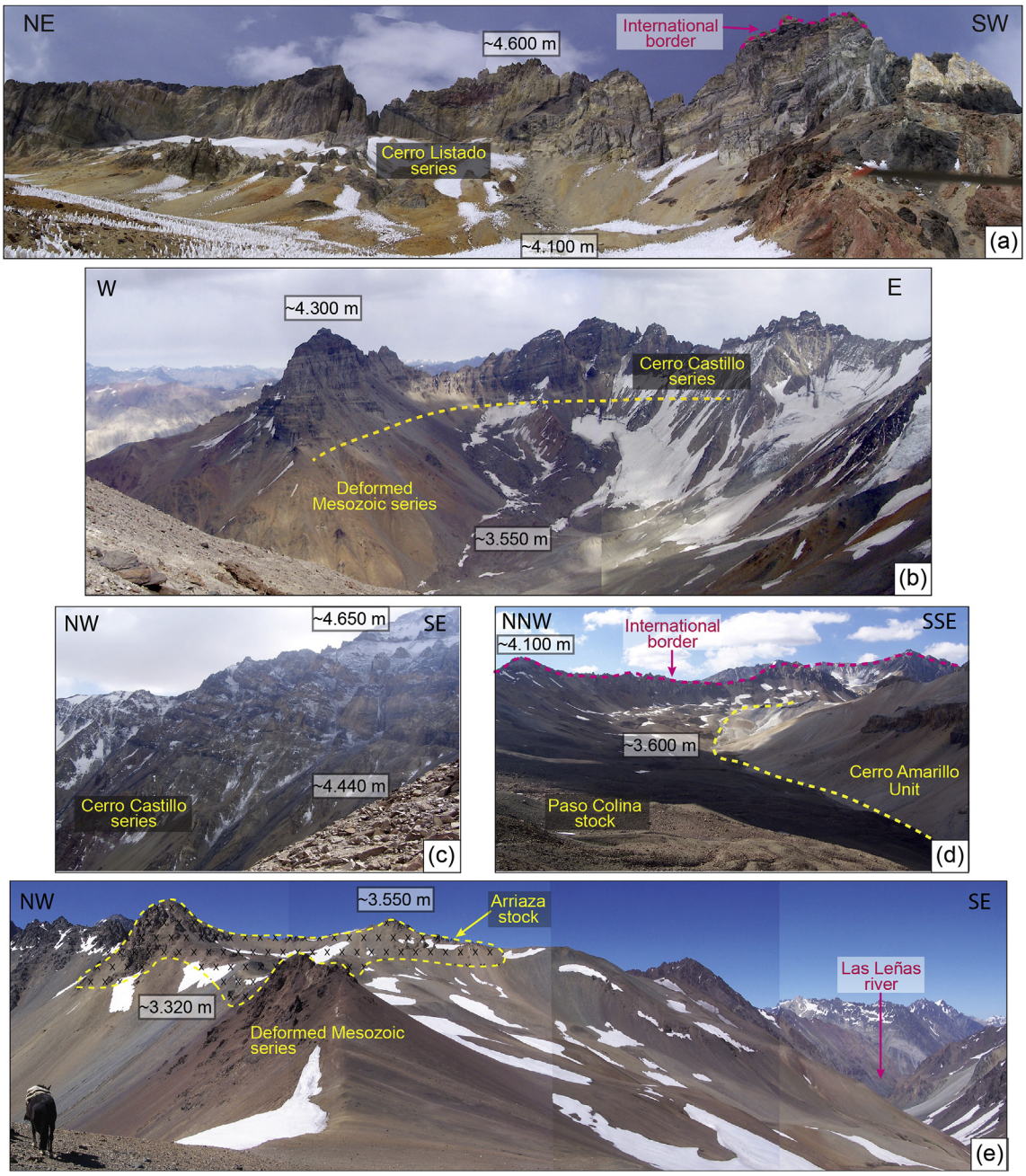

Fig. 2. Main outcrop characteristics of igneous units studied. These represent the late Pleistocene activity of the northern segment of the Southern Volcanic Zone of the Andes (NSVZ) and correspond to: (i) the inactive and eroded centers of Cerro Listado (a; ~34.15′S), Cerro Castillo (b, c; ~33°57′S), and Cerro Amarillo (d; ~33°52′S), and (ii) the intrusive stocks Paso Colina (d; ~33°51′S) and Arriaza (d; ~34°25′S). Approximate altitudes are indicated for reference. See Fig. 1 for locations and the main text for further details.

(Fig. 2a, b, c). In the Cerro Castillo and, less markedly, Cerro Listado series the lava flow package is characteristically composed of an alternance of dark and light colored obsidian and porphyric facies (Fig. 2a, b, c), respectively, both dacitic to rhyolitic in composition (see the following). In addition, and in particular for the Cerro Listado unit, an intense hydrothermal alteration can be locally observed in these eroded centers (Fig. 2a). It must be noted that all the mentioned characteristics were also observed in the field for the Picos del Barroso unit, yet difficulties in access made this series impossible to sample for further studies. In this work, Ar-Ar radiometric determinations were performed in bulk plagioclase samples from Cerro Castillo and Cerro Listado lavas (Fig. 3; Supplementary Material Item 1). Results indicate late Pleistocene ages, with 534 ± 185 ky for the Cerro Castillo (MM5; all errors reported at 2σ level; Fig. 3) and 319 ± 54 Ky for the Cerro Listado (MM14; Fig. 3).

Our sampling of volcanic rocks for laboratory studies returned only dacites and rhyolites from the units Cerro Castillo (n = 3) and Cerro Listado (n = 21). In terms of mineral phases, these rocks show a ubiquitous presence of plagioclase, pyroxene is very common, there is a variable presence of potassic feldspar, amphibole, biotite and clinopyroxene, and common accessory phases correspond to zircon and apatite (Fig. 4). The rocks show aphanitic to mildly porphyritic and vitrophiric textures and their fine grained portion presents traquitic and/or felsitic textures (Fig. 4). The development of perlitic and flow banding textures is common in the vitrophiric rocks (Fig. 4). All studied samples show disequilibrium features as glomerocrysts and/or crystal clots, and sieve, zonation and

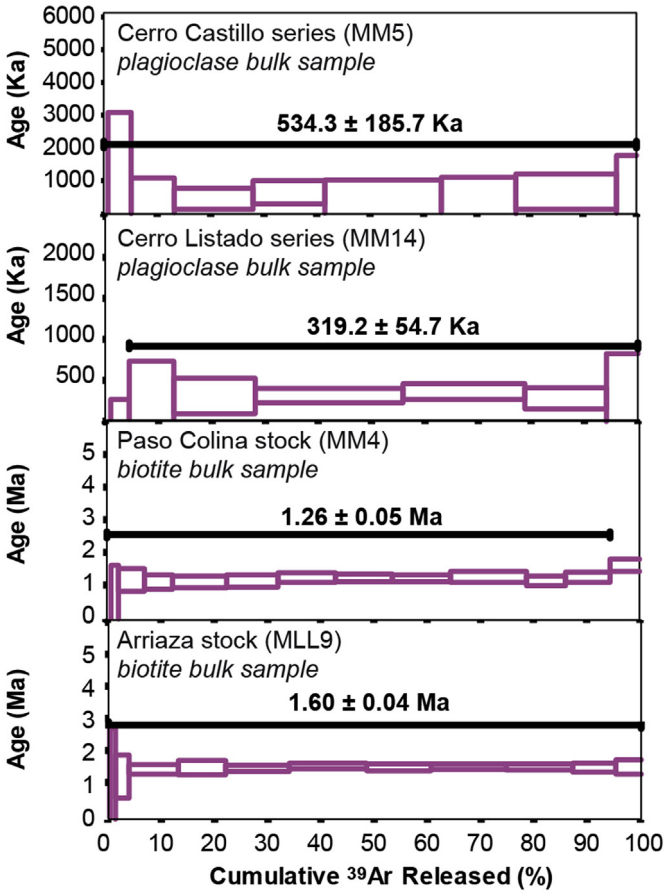

Fig. 3. $^{40}Ar/^{39}Ar$ ratio spectra obtained on plagioclase and biotite bulk samples. Samples and mineral concentrates analyzed, and plateau ages obtained, are indicated within each diagram. Thick black horizontal line in each diagram indicates the plateau used for age calculation.

embayed textures in plagioclase phenocrysts (Fig. 4). We determined mineral chemistry in the same samples with Ar-Ar radiometric analyses, an orthopyroxene rhyolite from Cerro Castillo (MM5) and a biotite rhyolite from Cerro Listado (MM14; Supplementary Material Item 2). Overall, the common and most abundant plagioclase composition corresponds to andesine, with a subordinated presence of labradorite and oligoclase (Fig. 5). In both samples, plagioclase phenocrysts show the more Ca-rich compositions and they usually show a normal zonation of up to 25% variation in Ca content between the cores and rims (Fig. 5). Plagioclase microlites are comparatively Ca-poor phases and correspond to andesine and alkaline feldspar respectively in samples MM5 and MM14 (Fig. 5). Orthopyroxene present in sample MM5 corresponds to enstatite and shows a restricted range in compositions (Supplementary Material Item 2). Phenocrysts phases develop a slight normal zonation and, in comparison to these, microlites correspond to more ferrosillite-rich members.

4.1.1.2. Cerro Amarillo. The Cerro Amarillo unit has been reported in a few studies (Thiele, 1980; Schneider et al., 1988; Ramos et al., 1997) but the only detailed description and compositional characterization was given by Godoy and Hildreth (2001). As indicated by the authors, this corresponds to a medium size (~500 m high, 2 km^2) rhyolite dome complex, composed by two units, which overlies a deformed Mesozoic series (Figs. 1 and 2). The older unit corresponds to a lava-pyroclastic sequence that includes collapse breccias, pyroclastic flows, banded rhyolite flows and fallout deposits, all of which are crystal poor bearing only plagioclase and biotite (Godoy and Hildreth, 2001). The younger unit includes vesiculated to massive black obsidian, finely laminated fallout deposits, and coarse grained biotite rich felsite (Godoy and Hildreth, 2001). Regarding its age, no radiometric determinations have been performed in rocks of the Cerro Amarillo unit. Originally, Thiele (1980) assigned it to the Old Volcanic Unit, the formal grouping in the region of the NSVZ units which immediately predate the modern volcanics. Later, Ramos et al. (1997) associated the Cerro Amarillo rocks with a series of felsic stocks and dikes, along with felsic extrusive pyroclastic facies, that crop out in the nearby regions both in the Chilean and Argentinean slopes of the Andes. Two K-Ar ages of ~3.5 Ma were obtained in the Argentinean units and thus Ramos et al. (1997) assigned all this felsic igneous activity to the late Pliocene. Afterwards, Godoy and Hildreth (2001) indicated that the Cerro Amarillo unit could not be older than Pleistocene based on the lack of younger overlying units, the freshness of its components, and the preservation of the unconsolidated, easily eroded pyroclastic deposits at its base. Tentatively, the authors suggested an age between 0.1 and 0.5 Ma.

Further constraints on the age of the Cerro Amarillo unit can be inferred from its field relations. The outcrops of this mainly extrusive facies unit are limited immediately to the north and east, in a nonconformity contact relation, by the outcrops of the Paso Colina stock (described in the following sections; Figs. 1 and 2). For the latter unit an age of ~1.2 Ma has been obtained in this work in this same location (Fig. 1). Moreover, while the Cerro Amarillo unit reaches an altitude of 4.162 m, the outcrops of the Paso Colina stock reach nearly 250 m higher and thus its summits compose the international border in this area (Figs. 1 and 2). These observations indicate that the Cerro Amarillo unit is definitely younger than 1.2 Ma and also probably younger than 1 Ma, as crystallization and exhumation of the Paso Colina stock must have proceeded before the emplacement of the Cerro Amarillo extrusive and subvolcanic facies.

4.1.1.3. Diamante Caldera and associated ignimbrite. This silicic latest Pleistocene stage (~0.1–1 Ma) of the NSVZ also encompasses the formation of the Diamante tuff, a rhyolitic, non-to moderately welded ignimbrite widely dispersed in westernmost Argentina and in Chile (Stern et al., 1984a). This unit includes pyroclastic flow deposits and associated fallout tuffs totaling an estimated volume of 260–450 km^3 (Stern et al., 1984a; Guerstein, 1993; Troncoso, 2012). Its genesis has been related to the formation of the 20 × 16 km^2 Diamante caldera over which the modern Maipo volcano sits (Fig. 1b; Polanski, 1962; Stern et al., 1984a, 2007; Wall et al., 2001). Overall, the unit corresponds to a massive and poorly consolidated deposit, with a ~40–90% ash size matrix, showing a highly vesiculated pumice component and a low crystal content (Stern et al., 1984a; Lagos, 2003; Troncoso, 2012).

The age of the Diamante tuff is a controversial issue. This might result in part from the combination of two factors: (i) the wide and dispersed nature of the deposits and (ii) the fact that, in this active volcanic region, mostly every poorly consolidated pyroclastic deposit found has been assigned to the Diamante tuff unit. Originally, Polanski (1962) assigned a late Pleistocene age to this unit based on stratigraphic criteria, which was later confirmed by an age of ~0.45 Ma obtained by Stern et al. (1984a) through the zircon fission track method. From then on younger and older ages have been reported for these deposits. Wall et al. (2001) obtained Ar-Ar plateau ages in biotite concentrates of ~1.4–2.2 Ma, Lara et al. (2008) reported a zircon U–Th–He age of ~0.15 Ma, and Ormeño (2007) reported Ar-Ar ages of ~0.32–0.36 Ma. Ultimately, Pineda (2015) performed U–Pb age determinations in single zircon crystals from 11 samples of the Diamante tuff deposits dispersed in Central Chile (33°-34°S). The author showed the significative

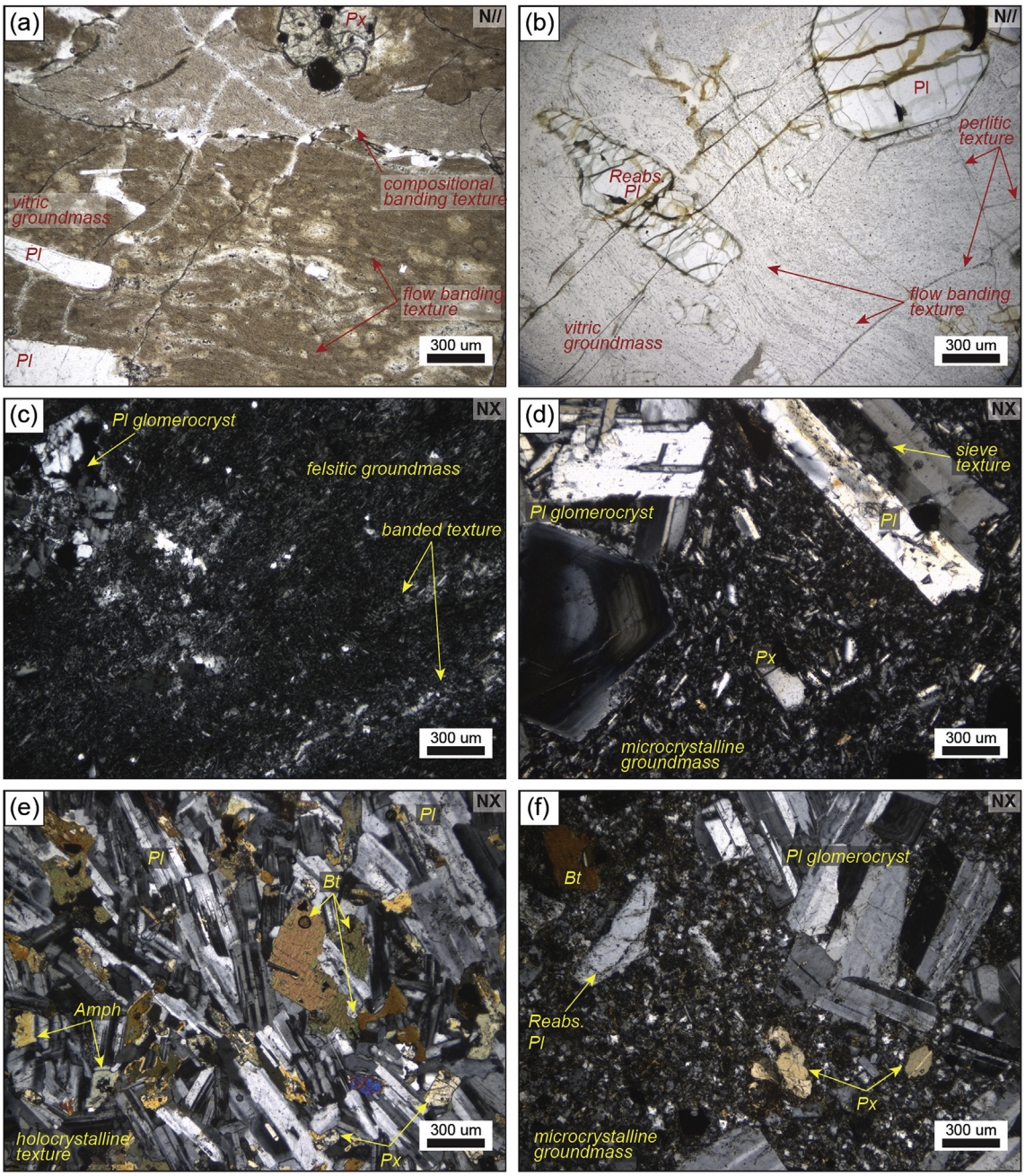

Fig. 4. Photomicrographs illustrating the main petrographic characteristics of the studied igneous rocks. Displayed samples correspond to felsic igneous volcanic rocks from the units Cerro Listado (a, b, c) and Cerro Castillo (d), and the intermediate stocks Arriaza (e) and Río Colina (f). Pl: plagioclase; Px: Pyroxene; Amph: amphibole; Bt: biotite; Reabs.: reabsorbed; N//: plane-polarized light; NX: cross-polarized light.

presence of inherited old components and, from the full composite data, she highlighted the two youngest age populations. The oldest of these corresponds to 0.39 Ma, a component present in all samples, and the youngest corresponds to 0.13 Ma, which is present in a single sample. For these results, the preferred explanation of Pineda (2015) was that the latter would correspond to the eruption age and the former would correspond to an earlier episode of zircon formation. From all the data presented, it is evident that the age of Diamante tuff is a problem far from being solved. In any case, it is also clear that this rhyolitic explosive episode (episodes?) occurred some time between 0.13 Ma and 0.86 Ma, the latter which corresponds to the earliest post-caldera lavas of the modern Maipo volcano (Sruoga et al., 2005, 2012).

4.1.2. Earlier stages (>1 Ma): intrusive arc units

Respect to the previous stage described, immediately older activity of the NSVZ seems to be represented only by intrusive units. Along the same arc area two units with ages of ~1.2 and ~1.6 Ma have been reported (Fig. 1b; Muñoz et al., 2013). The youngest of these is the Paso Colina stock which is exposed at 3.840 m, along the drainage divide, limiting to the north and east the outcrops of the Cerro Amarillo unit (Figs. 1b and 2d). This stock corresponds to an amphibole diorite for which we report an age of 1.26 ± 0.05 determined by Ar-Ar in biotite bulk sample (Fig. 3; Supplementary Material Item 1). The other unit corresponds to the Arriaza stock which is exposed at 3.380 m, immediately to the west of the drainage divide, nearly 12 km to the south of Picos del Barroso and Cerro Listado units (Figs. 1b and 2e). This stock corresponds to a

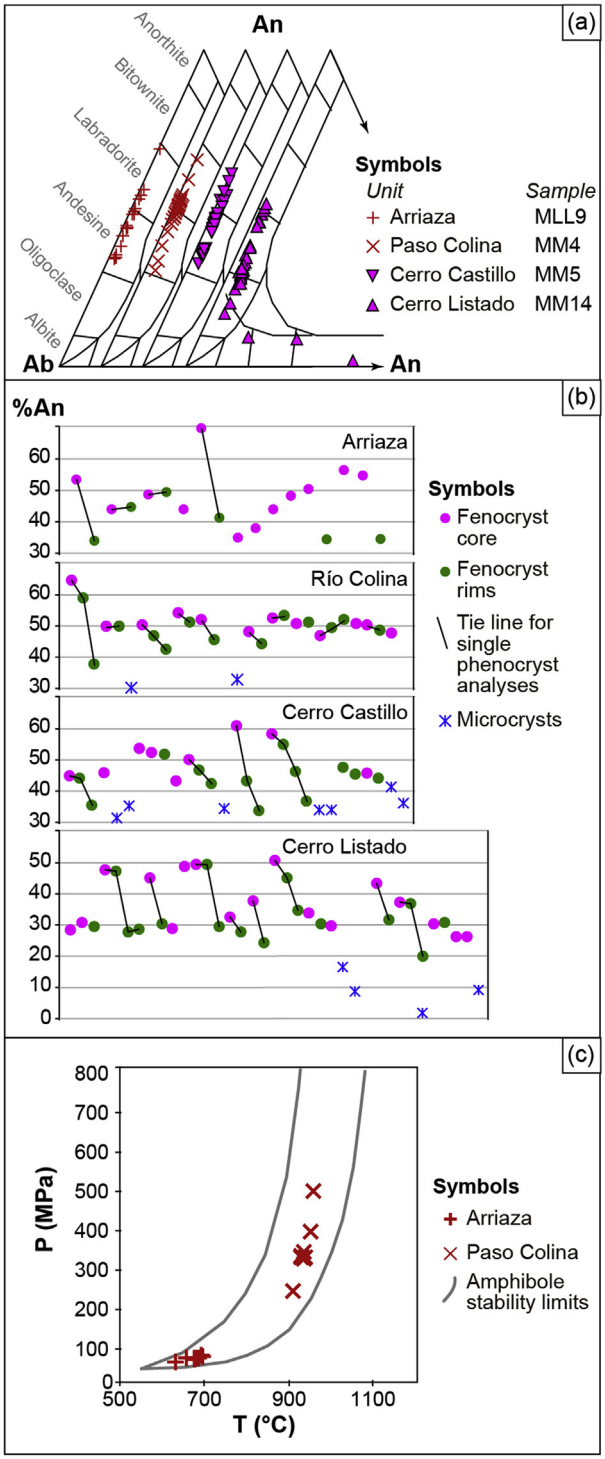

Fig. 5. Results from mineral chemistry analyses and calculations for the studied samples. (a) Plagioclase classification scheme. (b) Diagrams illustrating the compositional variation within and between plagioclase crystals in each sample. (c) Results of amphibole thermobaromerty using the calibration of Ridolfi and Renzulli (2012).

clinopyroxene diorite for which we determined an age of 1.60 ± 0.04 by Ar-Ar determinations in biotite bulk sample (Fig. 3; Supplementary Material Item 1). An additional intrusive unit with similar young ages in the region corresponds to the Los Lunes stock which crops out nearly 20 km to the west of the area occupied by the current NSVZ (Fig. 1b). This corresponds to a biotite andesitic stock, emplaced in a Cenozoic stratified series, for which Godoy (1998) reported an age of 1.1 ± 0.4 Ma (K-Ar in biotite bulk sample).

According to our macroscopic and microscopic petrography, all mentioned stocks correspond to holocrystalline and weakly porphyritic rocks composed of plagioclase, lesser amounts of amphibole and biotite, and accessory apatite and zircon (Fig. 4). Pyroxene crystals are also present in the Arriaza unit where they occasionally conform scarce glomerocrysts. In these units a small proportion of the plagioclase crystals show well developed disequilibrium features as zonation patterns and reabsorption textures. We determined mineral chemistry in the same samples with Ar-Ar radiometric determinations of the Paso Colina (MM4) and Arriaza (MLL9) units (Fig. 3; Supplementary Material Item 2). For both samples, plagioclase composition ranges between labradorite and andesine and the observed zonation is commonly normal, and scarcely reverse, and can reach up to 25% variation in the Ca content between the phenocrysts cores and rims (Fig. 5). Biotite and amphibole show fairly homogeneous compositions. According to Mg/(Mg + Fe_t) and Al^{VI} contents, biotite minerals correspond to phlogopite in both samples. According to the Leake et al. (1997) classification scheme, amphibole minerals correspond to pargasite in the Paso Colina stock and Mg-hornblende in the Arriaza stock. This latter unit also contains unzonned ortho- and clino-pyroxenes corresponding respectively to enstatite and augite.

Both the presence of amphibole and the compositions determined for this mineral phase make Paso Colina and Arriaza stocks susceptible for thermobarometric determinations based on mineral chemistry. In this work the calibration of Ridolfi and Renzulli (2012) has been used for calculating the temperature and pressure of amphibole crystallization and the full results are presented in the Supplementary Material (Item 2) and summarized in Fig. 5c. The 16 amphibole analyses fulfill the calibration criteria and they correspond to 8 for each unit. For the latter data, all obtained P-T results fall within the amphibole stability curve and thus they can be considered valid for this calibration (Fig. 5c). For the Paso Colina stock calculated pressures range mostly between 3.1 and 3.8 kbar (6 analyses), with 2 extreme values of 2.3 and 4.5 kbar, and calculated temperatures range between 908 and 957 °C (Fig. 5c). For the Arriaza stock pressure and temperature estimates vary respectively between 0.5 and 0.7 kbar and 632–693 °C (Fig. 5c). Considering a crustal geobarometric gradient of 0.33 kbar/km, estimated pressures correspond to equivalent depths of ~9–12 km for the Paso Colina stock and ~1.5–2.0 km for the Arriaza stock. For the Paso Colina stock, P-T results indicate that amphibole crystallization occurred early in magmatic evolution and deeper than the location of the final reservoir where this stock lastly emplaced to complete crystallization. These observations are based in both the high temperatures above the hydrous solidus of an andesitic melt (~700 °C) and the fact that such unit is currently exposed and more than 2.5 km of exhumation in the area are unrealistic given the estimations for this region in the last ~1 m.y. (Farías et al., 2008). For the Arriaza stock, P-T estimations probably reflect amphibole crystallization in the last and upper magmatic reservoir which currently corresponds to the exposed intrusive unit. This inference is supported by the low temperatures obtained for this basaltic andesitic unit which indicate near solidus conditions.

4.1.3. *Main compositional characteristics and its variations in time*

Compositional characteristics of the units previously described, in terms of whole rock major and trace element geochemistry and Sr-Nd isotopic composition, are reported in scarce previous studies (Stern et al., 1984a; Godoy and Hildreth, 2001; Baker et al., 2009) and this work (Table 1). In addition, the composition of the currently active centers of the NSVZ has been more extensively addressed in several works (e.g. Stern et al., 1984b; López-Escobar et al., 1985; Hildreth and Moorbath, 1988; Futa and Stern, 1988;

Sruoga et al., 2005, 2012; Holm et al., 2014). From all the data reported, such active centers define a basaltic andesite-andesite-dacite suite ranging in silica contents between ~53 and 68% (all values given at anhydrous basis; Fig. 6a). Comparatively, a striking difference is observed in the compositions displayed by units from the latest Pleistocene stage (0.1–1 Ma). These are markedly more differentiated, defining exclusively a rhyolite suite, as shown by SiO_2 contents between ~71 and 80% (Fig. 6a). Immediately earlier stages, represented by the 1–1.6 Ma intrusive arc units, show SiO_2 contents between ~54 and 62% which are fully contained in the basaltic andesite-andesite-dacite suite described by the current NSVZ volcanics (Fig. 6a and b). Moreover, similar compositions are also displayed by all previous igneous units in the area which show a range of SiO_2 contents between 55 and 65% up to at least 8 Ma

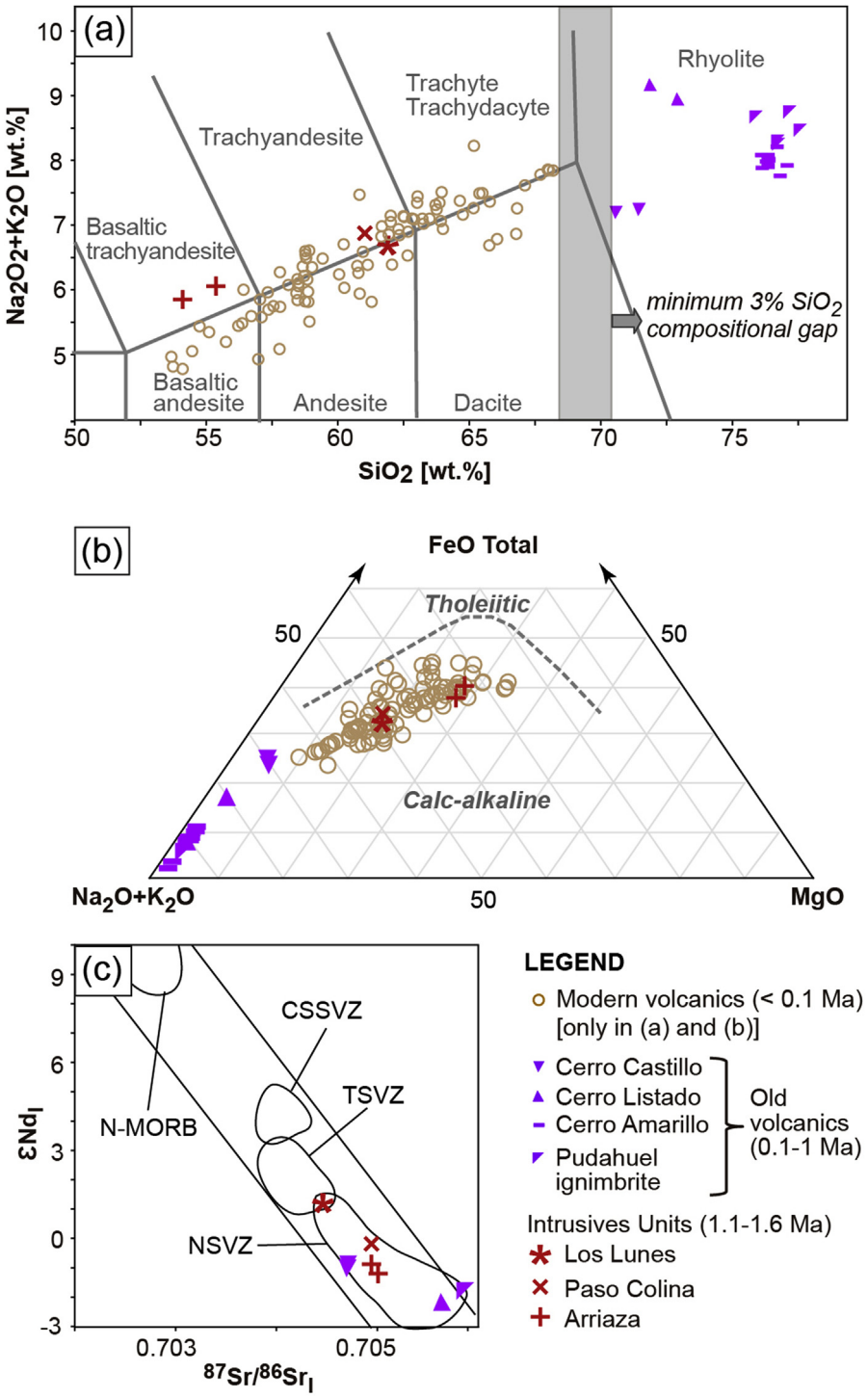

Fig. 6. Main compositional characteristics of the Quaternary igneous activity of the NSVZ: (a) TAS diagram, (b) AFM diagram with the calc-alkaline and tholeiitic subdivision according to Irvine and Baragar (1971), and (c) εNd_I versus $^{87}Sr/^{86}Sr_I$. Geochemical data for the SVZ taken from López-Escobar et al. (1985), Futa and Stern (1988), Hildreth and Moorbath (1988), Stern et al. (1984a, 1984b), Godoy and Hildreth (2001), Sruoga et al. (2005, 2012), Baker et al. (2009), Holm et al. (2014), and this work. Fields for the Sr-Nd isotopic compositional range of the CSSVZ and TSVZ compiled from Hickey-Vargas et al. (1986) and Kay et al. (2005). CSSVZ includes data from the Central and Southern portions of the SVZ (south ~37°S).

(Muñoz et al., 2013).

Following the previous observations, the latest Pleistocene stage of the NSVZ constitutes a distinct silicic episode for this arc segment and this even defines a 3% gap in silica contents respect to previous and later igneous units (Fig. 6a). Noticeably, in terms of major element composition altogether the units describe coherent patterns of covariation (*liquid line of descent*) which suggest differentiation through crystal fractionation processes and thus links of the full compositional spectra (Fig. 6a and b). In terms of the Sr-Nd isotopic signature all these Quaternary igneous units define a single coherent group showing no variation between the different compositions considered (Fig. 6c), a feature that strongly arguments for a cogenetic relation amongst them. Most importantly, this indicates that the compositional changes recorded through time are related to late magmatic processes, once the base signature has been established (*sensu* Hildreth and Moorbath, 1988), namely in the upper crustal magmatic reservoirs feeding the arc volcanoes.

4.2. Orogenic processes and the erosional response to uplift

Construction of the Andean orogen in the NSVZ area has followed an evolution characterized by crustal shortening and thickening and associated uplifting and denudation (e.g. Giambiagi and Ramos, 2002; Charrier et al., 2002; Farías et al., 2008, 2010). The altitude of the modern Andes is roughly isostatically balanced and the mountain range reached the current configuration by ~7-4 Ma (Giambiagi and Ramos, 2002; Farías et al., 2008). For the area hosting the active volcanic arc evidence indicates a rapid and high magnitude regional uplift, of between 1.5 to at least 2.5 km, based on equivalent incision measures in river valleys. However, the erosional response that the latter features represent was not coeval to the major uplifting event and its propagation into the area was delayed by several m.y. (Farías et al., 2008).

A few geologic markers place first order constraints on the arrival times and magnitudes of either river incision or unroofing/denudation processes into the Andean NSVZ region. Nearly 17 km downstream from the current volcanic chain, the ~1.1 Ma Los Lunes stock (Fig. 1b) crops out at almost 2 km above the bottom of the Volcán river valley and 500 m below the top of the hillslope. In addition, about 150 m above the river an ash deposit of the Diamante tuff (dated in ~0.3 Ma; Ormeño, 2007) covers a thin layer of fluvial deposits emplaced over a ~10 Ma pluton (Farías et al., 2008). These observations constraint ~1.9 km of incision that occurred between ~1.1 and 0.3 Ma and they also indicate that the eastern propagation of this into the current arc area occurred no earlier than ~1.1 Ma. Overall these estimations bracket an increased denudation event in the region which occurs mostly coevally with the latest Pleistocene stage of silicic magmatism developed in the NSVZ. Moreover, geologic evidence within the currently active NSVZ area, along the drainage divide, also points to similar results particularly in relation to several aspects of the 1.2–1.6 Ma stocks. Regarding the latter, it has to be considered firstly that the highest level of exposure of these intrusive units is higher than the basal level of the NSVZ volcanic series (active and extinct). This observation alone records a significant amount of unroofing of probably >1 km between both igneous events, an estimation further constrained when considering the emplacement depth of 1.6–2.2 km indicated by geobarometric calculations over the currently exposed Arriaza stock (Figs. 1b and 5c). In addition to the latter, features as the onlap contact relation of lavas from the Cerro Amarillo unit (0.1–0.5 Ma) with the Paso Colina stock (~1.2 Ma) indicate that most denudation occurred between both igneous events lasting at the most until the age of the former unit. Overall, all these observations indicate that the increased denudation event in the NSVZ area would have arrived after 1.1 Ma and lasted at the most up to the formation of old volcanic edifices.

A few considerations must be discussed regarding the role of glaciation events in the erosional processes described above. Glaciated morphologies are evident in the high Andes in the study region and numerous of these events have occurred throughout Quaternary in the area. It has to be noted first that the NSVZ segment, distributed between ~33° and 34°30′S, lies at significantly northern latitudes respect to those expected to be covered by an ice cap during Quaternary glaciation periods. For example, records of the Last Glacial Maximum (LGM) indicate that the Patagonian ice sheet extended continuously between 56° and 37°S and discontinuously further north, until up to ~32°-33°S, it was probably represented by mountain glaciers confined to higher altitude areas (e.g. Rabassa et al., 2005; Watt et al., 2013). This configuration probably dominated the study area through all glaciation events in the last 1 Ma at least. The largest of these events documented in the Southern Andes corresponds to the Great Patagonian Glaciation (GPG), which occurred at ~1 Ma (Mercer, 1976; Rabassa et al., 2005 and references therein). Rabassa et al. (2005) indicated that a first order valley deepening event took place after the GPG as later glaciations (<0.8 Ma) were forced to develop a morphology of discharge glaciers entrenched in their valleys. According to these authors, the much larger magnitude of deepening between GPG deposits and later glaciation events, compared with that between the latter, suggests a tectonic uplift origin for this canyon-cutting event (*sensu* Rabassa and Clapperton, 1990; Rabassa and Evenson, 1996). These timings tightly fit with the arriving of the increased erosion event to the high Andes documented in our study region, which is bracketed as post- 1 Ma and pre-0.1 Ma. All these considerations favor a model of morphological evolution first dominated by the establishment of incision valleys which are later further deepened and shaped by both glacial erosion and tectonically induced increased erosion. Under this scheme, and at scales of hundred thousand years, it can be considered that both processes operate together constructively in the increased erosion event recorded in the region during the last 1 m.y.

5. Numerical modeling: pressure constraints over magmatic evolution

5.1. Conceptual frame and modelling constraints

In order to assess the impact of increased denudation over the magma composition and volatile content, we have performed several numerical models on crystallization of representative samples of the Andean Quaternary arc (all displayed in the TAS diagram of Fig. 7). This was done by using the Rhyolite MELTS thermodynamic software (Gualda et al., 2012; Ghiorso and Gualda, 2015). Given that subvolcanic magma reservoirs are inferred to stall at upper crustal levels, and a conservative estimation of denudation of ~1.5 km, we have considered a range of pressures between 2 and 0.1 kbar (ca. ~6 to 0.3 km of equivalent rock column). For the analysis, and as it is illustrated in the figures, this range has been subdivided in a series of pressure steps. Each simulation ran provides the chemical evolution, the crystallinity fraction and the volatile solubility as the magma crystallizes at a certain pressure condition (isobaric), with temperature steps of 0.5 °C and an oxygen buffer QFM+2, from an initial composition chosen from the data of the Andean Quaternary arc (Fig. 7). In our models it is implicit that the compositional trend of the whole arc can be replicated from the crystallization of less differentiated samples (Fig. 7), which is adequate for evaluating the effects of geodynamic processes over the magmatic evolution at regional scale and is in turn supported by the coherent patterns displayed by the NSVZ geochemical data. Given the variably porphyritic nature of Andean arc volcanic rocks, these same regional scale considerations should

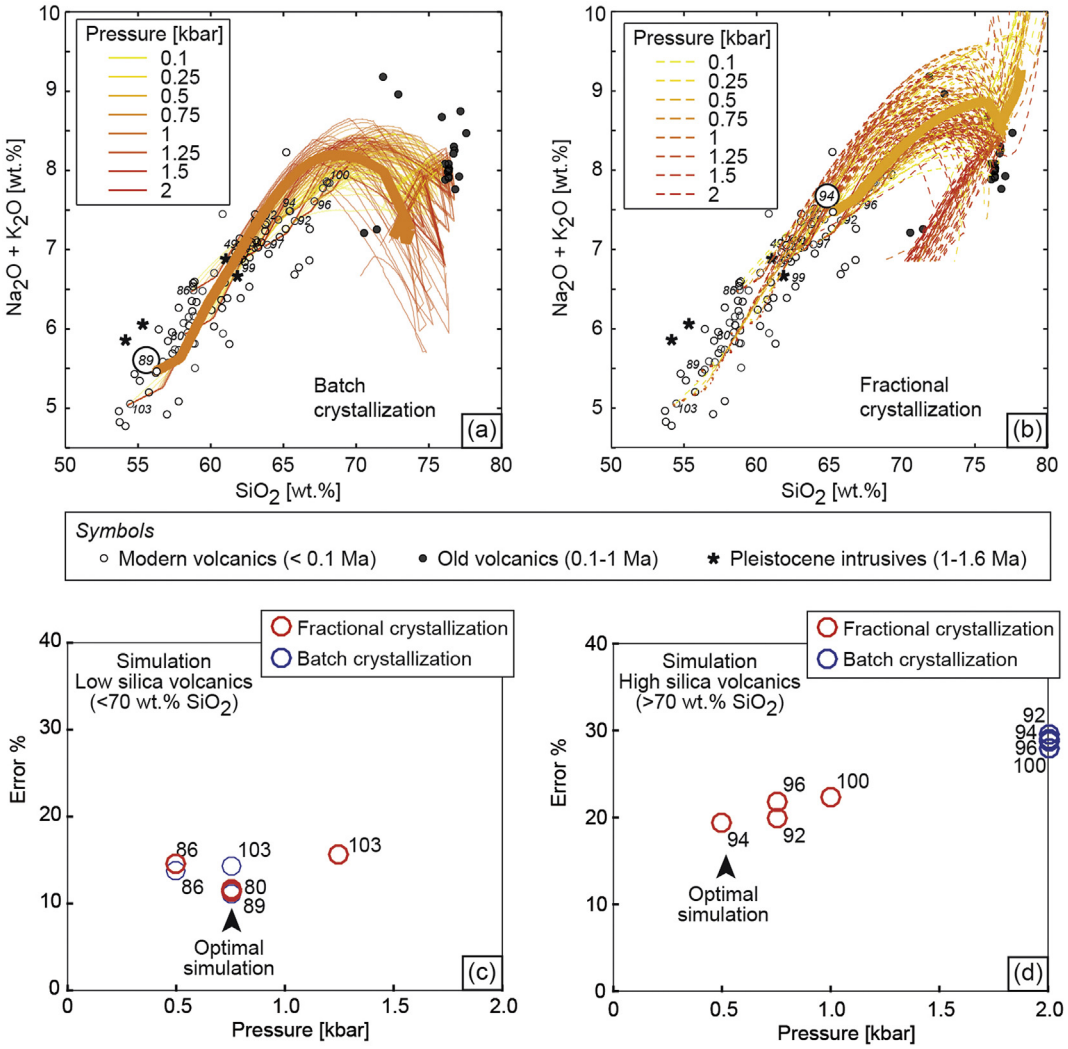

Fig. 7. Main results of numerical simulations for describing the compositional trends of the NSVZ Quaternary arc. The upper plots display the simulations for crystallization in (a) batch and (b) fractional modes over a TAS diagram. Starting compositions are taken from 14 selected samples of this arc segment and simulations cover the different pressure values discussed in the text. Geochemical data of the NSVZ as in Fig. 6. The lower plots display the mean absolute percent difference (Error %) of different simulations (starting compositions) for their optimal pressure condition (those that minimize the error for each composition). These plots are separated in the cases of the (c) low silica (SiO_2 <68%) and (d) high silica groups. In (c) only samples with SiO_2 <61% were considered as starting compositions, all the major elements were considered in the simulations, and results of batch and fractional crystallization show no major differences. Compositions were replicated with the minimum error by both batch and fractional crystallization of sample 89 (SiO_2 = 56.4%) at 0.75 kbar (see a, b). In (d) only compositions with SiO_2 contents between 63 and 66% were considered, as suggested by the compositional gap of this arc segment, and results for fractional crystallization show systematically lower associated errors than results for batch crystallization. Compositions were optimally replicated with the minimum error by fractional crystallization of sample 94 (SiO_2 = 65.4%) under 0.5 kbar.

also overcome the fact that the NSVZ compositions used in our simulations are probably not true liquids in most cases. As shown in Fig. 7, numerous simulations were run from different starting compositions which overall reproduce the compositional trend displayed by the NSVZ Quaternary arc. Afterwards, a statistical analysis based in error minimization was carried out to assess the most representative simulation (pressure value P and initial composition X_0) of the compositional trend of the arc. Thus, we selected the simulation whose liquid line of descent minimizes the mean relative error (least square method) respect to the compositions of the NSVZ samples defining the mathematical optimal physical conditions. All initial compositions considered in our models and discussed in the text and figures are included in the Supplementary Material Item 4.

The statistical analysis of the simulations must be consistent with considerations about the geological and physical processes during magma differentiation, which are imposed in order to choose a geologically meaningful starting composition. In consequence, such analysis for simulations representing the arc segment is addressed through a forward approach, according to criteria listed in the following. This has been applied and discussed in the next section describing the overall results from numerical simulations.

(i) The best starting point to reproduce the compositions of the arc segment was calculated by minimizing the error of simulations from starting compositions lower in SiO_2 contents than the compositional trend to be reproduced. This means that, for example, to reproduce samples with silica contents between 60 and 68%, the starting point must present silica contents equal or lower than 60%.

(ii) The melt composition must be reached when the magma is in a crystallinity stage that makes possible magma transport or melt extraction processes. This means that the magma crystallinity has to be below or within the crystallinity window for optimal melt extraction of 55–60% (Dufek and Bachman, 2010; Aravena et al., 2017).

(iii) Under the last condition, if the target composition is reached under higher crystallinity values than the optimal crystallinity window for melt extraction, some melt fractionation event should have had to occur to explain the genesis of the more silicic samples. Subsequently, the silica content when the optimal extraction crystallinity window is reached is considered as starting composition to reproduce the high-silica samples, applying the method described in the first stage.

5.2. Compositional trends and initial compositions for the NSVZ quaternary arc

In general, simulation results indicate that the compositional spectra displayed by the NSVZ Quaternary arc can be linked by differentiation processes through crystallization (Fig. 7). There is however a higher dispersion in elements as alkalis for the more differentiated compositions (SiO_2 >71%; Fig. 7), which is probably the combined result of: (i) the high pressure dependence of crystallization of phases that include alkali elements, and (ii) the high mobility of the latter in alteration processes.

The lower silica compositions, represented by samples with SiO_2 <68%, are well reproduced both by batch and fractional crystallization of the less differentiated samples (SiO_2 <61%; Fig. 7a) and simulations show mean relative errors between 10 and 15% (Fig. 7c). For the latter parameter all the major elements were considered (SiO_2, TiO_2, Al_2O_3, FeO_T, MgO, CaO, Na_2O, K_2O), and only FeO_T, MgO and TiO_2 present higher errors between 20% and 30%. Crystallization of sample 89 (indicated in the figures), from the Maipo volcano, reproduces the compositional trend optimally at 0.75 kbar by fractional crystallization and batch crystallization (error of 10.8%; Fig. 7c). Noticeably, this result supports our hypothesis that the recorded magmatism evolved in shallow levels in the crust, between 1.5 and 3 km depth, and suggests that the evolution of the basaltic andesite-andesite-dacite suite of this arc segment can be fairly represented by this compositional trend.

For analyzing the simulation results that replicate the high silica compositions (SiO_2 >71%) we considered all the mentioned oxides excepting TiO_2 and CaO. The latter are not well replicated by MELTS because phases as apatite are not considered in crystallization assemblages. The most silicic compositions of this group are represented by the Diamante ignimbrite and the Cerro Amarillo rhyolites (Fig. 6a). According to simulations, these could be replicated by batch and/or fractional crystallization of less differentiated samples (SiO_2 >61%), which occurs mostly close to the eutectic of the system (Fig. 7a and b). Through batch crystallization such high-silica melt compositions (SiO_2 >71%) are achieved at crystallinity values higher than 60% which makes melt extraction processes unlikely. This result suggests that, in order to reach the highly evolved compositions from the less differentiated samples, fractionation events have had to occur throughout the magma evolution. Simulations of fractional crystallization from intermediate samples (SiO_2: 63–66%) under pressures between 0.5 and 1 kbar minimize the error, which shows values between 19 and 24%, and the best fit is obtained for sample 94 optimally at 0.5 kbar with an error of 19% (Fig. 7d). As mentioned before, this supports both of our hypotheses, that fractionation processes governed the magmatic evolution to reach the most differentiated compositions and that crystallization processes occur mostly in the shallow crustal reservoirs feeding the arc volcanoes.

5.3. Magmatic evolution path and evaluation of pressure effects

Summarizing the results of the previous analysis, a magmatic evolution path that optimally reaches the compositional features of the most silicic volcanics of the NSVZ Quaternary arc can be established. Overall this can be described by two crystallization stages, separated by a fractional process, where the second stage evolves from the melt extraction of interstitial melts from the previous stage (Fig. 8). Such mixed scenario is supported statistically and is also geologically meaningful. Excepting for the silicic episode, the arc has been able to produce consistently compositions up to SiO_2 ~68% (Fig. 6a), whether under equilibrium and/or fractional processes (Fig. 7), and this should be representative of the most evolved feeding reservoirs. In addition, the gap observed between 68 and 71% SiO_2 contents argues for a fractional process linking the whole compositional range (Figs. 5 and 6). Moreover, the optimal magmatic evolution path obtained also fulfils several geological and physical processes that occur during magma differentiation, as described in the following. It must be noted, however, that our general observations apply to numerous of the mixed scenarios that can also explain the compositional features of this arc segment (Fig. 7).

Throughout magmatic evolution, reaching the high silica compositions is primarily dependent on crystallinity, a parameter that shows only minor variations among different pressure conditions (Fig. 8b). The equilibrium crystallization scenario from the most basic samples shows that silicic compositions with SiO_2 >71% are reached since crystallinities between ~60 and 70%, but the most evolved compositions observed (SiO_2 ~77%) cannot be reproduced (Fig. 8b). For magmatic reservoirs that have evolved to homogeneous mushes, this crystallinity value is in the window for optimal melt extraction (~50–70% crystallinity; Dufek and Bachman, 2010; Aravena et al., 2017), that is when crystals start forming a connected network with interstitial melt and the magma reaches the rheological transition from liquid to solid (Bachmann and Bergantz, 2004; Dufek and Bachman, 2010). In this situation the likely case for explaining the most evolved compositions is a fractionation process, which can occur since SiO_2 contents of ~65% that are attained from 50% crystallinity onwards (Fig. 8b). This suggests a halfway fractional process linking the whole compositional range and also accounts for the gap observed between SiO_2 ~68–71%. Compositionally, this evolution is replicated under different constant pressure conditions because the SiO_2 content of melts is primarily dependent on the crystallinity of the magma (Fig. 8b). Following fractionation from the previously segregated melts, silicic compositions with SiO_2 >71% are then reached since ~10% crystallinity, and further crystallization prompts the generation of progressively more silica rich melts until ~40% crystallinity when the system reaches the eutectic (Fig. 8b). As well as for any other compositionally similar arc system, the previous observations show that magmas from the Quaternary Andean arc have the potential to generate silicic melts, yet they do not explain by themselves the occurrence of a regional scale episode of silicic volcanism. The virtual absence of silicic compositions in the basaltic andesite-andesite-dacite suites of the arc, which occurs before and after the increased denudation event, shows that if such melts were generated they were unable to erupt. This is probably the result of an inefficient unmixing to mobilize the interstitial melt which would lead to: (i) eruption of magmas less silicic than the sole interstitial melt, thus generating a magmatic suite reaching up to only dacitic compositions, and (ii) solidification of intermediate composition intrusions at depth, as is actually seen in the 1.2–1.6 Ma stocks in the area (SiO_2: 54–60%).

Abrupt changes in pressure conditions of the magmatic system may prompt a sudden fractionation process, as that described above, along with volatile exsolution, both parameters that have a profound effect in the physical properties of magmas. According to simulations, crystallinity describes a steady increase with decreasing T, a behavior that occurs at progressively higher temperatures with decreasing pressure because the lower volatile

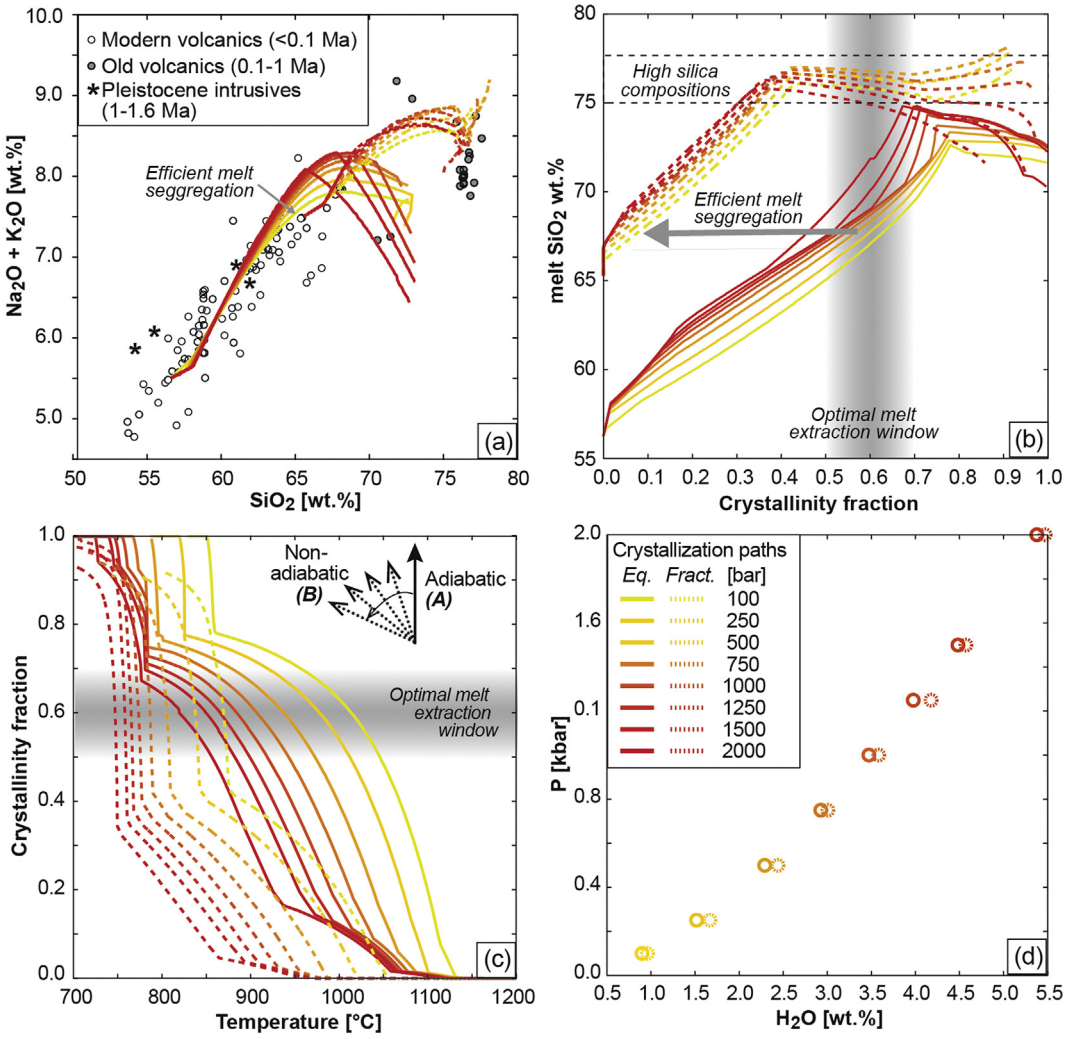

Fig. 8. Simulated evolution of magmas from the Northern Southern Volcanic Zone of the Andes (NSVZ). Parameters illustrated correspond to: (a) whole rock $Na_2O + K_2O$ vs. SiO2 [wt.%] (TAS diagram), (b) melt SiO_2 [wt.%] vs. Crystallinity fraction, (c) Crystallinity fraction vs. Temperature [°C], and (d) Pressure [kbar] vs. H_2O [wt.%] saturated melt content. The illustrated scenario involves two steps of crystallization, an equilibrium one (Eq.) followed by a fractional one (Fract.), separated by a fractional process. Initial compositions are taken from lavas of the NSVZ, respectively with SiO_2 contents of 56.4 and 65.4%, and they correspond to those that optimally describe the trends displayed by this arc segment (see the main text and Fig. 7). From each starting composition simulations describe the evolution under the different pressure conditions indicated in the inset in (d). Window for optimal melt extraction taken from Dufek and Bachman (2010) and Aravena et al. (2017).

solubility entails an increase in the solidus temperature (Fig. 8c and d). In this scenario, a sudden decrease in pressure at any point before solidification, whether as an adiabatic (path A in Fig. 8c) or non-adiabatic process (path B in Fig. 8c), will prompt the rapid generation of more silicic interstitial melts. This results from the rapid increase in crystallinity which is the main parameter that controls the SiO_2 content of the melt (Fig. 8b). We hypothesize that the extraction process is triggered in turn by the loss of volatiles from the magmatic system that proceeds along with decompression. Numerical simulations predict a degasification of ~1–2%, in the case of pure H_2O, in the adiabatic decompression scenario, for a maximum of 0.5 kbar (~1.500 m of rock column; Fig. 8d). The process itself can have a twofold effect: (i) favors gas-driven filter pressing processes that enhance crystal melt segregation (Sisson and Bacon, 1999; Bachmann and Bergantz, 2003, 2004), and (ii) favors wall-rock fracturing by fluid-pressure increase thus increasing the permeability for magma channelization and, if the volume of the magma reservoirs is enough, it may also promote the explosive volcanism.

6. Conclusions and final remarks

The Andean Arc in Central Chile shows a transient period of silicic magmatism (SiO_2 >70%) which is developed in latest Pleistocene (~0.1–1 Ma). This is recorded in several eroded and inactive arc centers, and its associated deposits, and is preceded and followed by magmatic activity corresponding to basaltic andesite-andesite-dacite suite compositions (SiO_2 <68%). This episode also occurs coevally to a period of uplifting and associated increased erosion event in the region for which conservative estimates of denudation of ~1.5 km are recorded in geologic markers in the field (e.g. Farías et al., 2008) and also supported by thermobarometric estimations in local intrusions.

We have evaluated through thermodynamic numerical simulations, under different pressure conditions, the evolution of NSVZ arc magmas at regional scale. Overall, results show that the compositional spectra defined by this arc segment can be reproduced by low pressure (<0.75 kbar) crystallization of its most basic members by batch and/or fractional processes. However, a rapid generation and extraction of silicic melts from intermediate

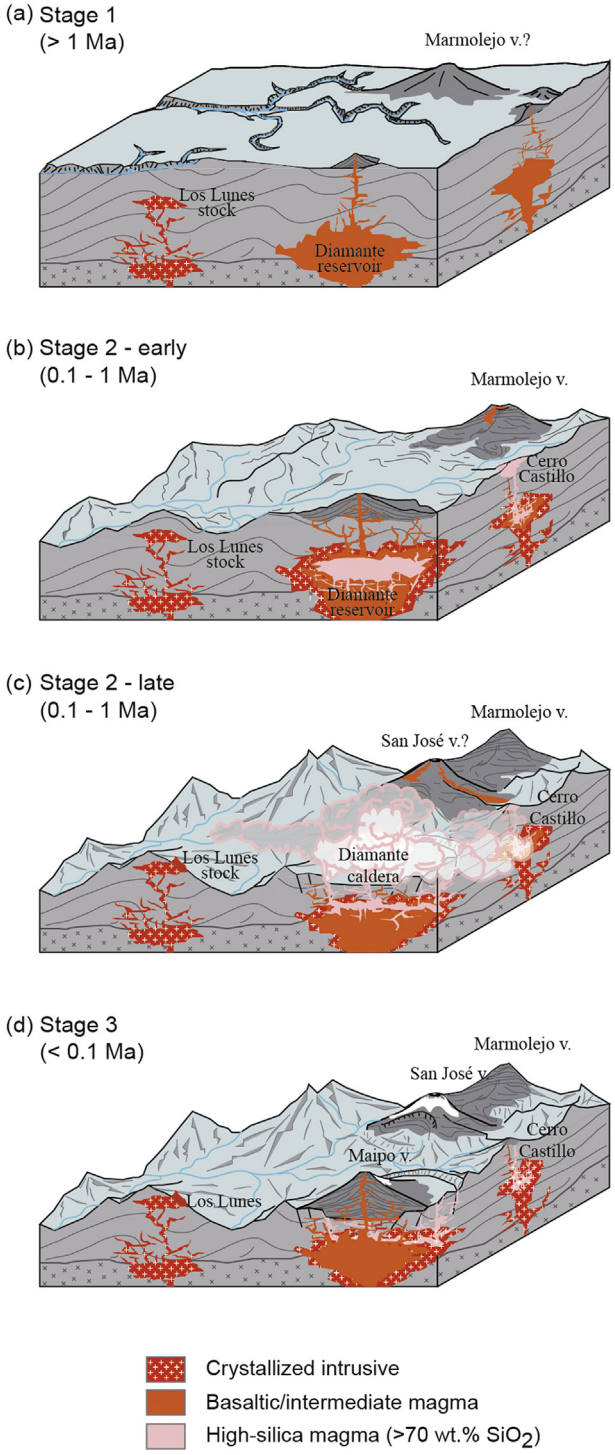

Fig. 9. Schematic illustration for the paleogeographic evolution of the Quaternary Andean arc of central Chile (33°50′-34°30′S). (a) The first stage (>1 Ma) is characterized by a stable geography where the basaltic andesite-andesite-dacite suite compositions characterize this volcanic arc segment. The activity derived from shallow reservoirs is illustrated along with those that speculatively derive from long lived, and probably deeply sourced, major volcanic centers as the Cerro Marmolejo. (b) The second stage (0.1–1 Ma) develops in response of an increased denudation event related to the main Andean uplifting event of the region. The associated disturbance of the shallow arc feeding reservoirs, as a sudden pressure decrease, prompts the generation of silicic magmas distinctively characterized by compositions with SiO_2 contents >70%. (c) Melt extraction from the shallow reservoirs is favored from devolatilization which in turn favors fluid-pressure increase in permeability for magma channelization. In the latter scenario, if the volume of the magma reservoirs is big enough this could also promote explosive volcanism as that represented by the Diamante ignimbrite. (d) After the surficial perturbation has ceased the magmatic system returns to its stable previous configuration which is compositionally characterized by the pre-1 Ma suite compositions.

compositions (SiO_2 ~65–66%) is needed to explain the most silicic compositions corresponding to the recorded transient volcanism event. Results also show that a sudden pressure decrease over the shallow magmatic reservoirs feeding the arc volcanoes creates a unique set of conditions that constructively operate for prompting such segregation event of a volatile saturated high-silica melt. The transient period of increased denudation in the region that follows from the uplifting can be considered as a superficial perturbation over magmatic reservoirs that should last only until the tectonic frame has reached again a stable state (Fig. 9). From there onwards, given that the magmatic factory from depth has remained unchanged, the whole shallow system of the arc should return to the previous regular configuration, as it is actually found in the return to the basaltic andesite-andesite-dacite compositional suite of the modern volcanoes (Fig. 9).

Considering the full NSVZ segment, a special mention has to be made about the Cerro Marmolejo center, a late Pleistocene volcanic complex located immediately to the north of our study area (Fig. 1). This unit remains poorly characterized, but the few studies performed in it report a predominantly andesitic nature for its volcanic products (Hildreth and Moorbath, 1988; González-Ferrán, 1995) thus constituting an exception to the regional silicic episode documented in this work. Cerro Marmolejo center is, however, fairly particular: (i) it corresponds by far to the longest-lived and largest center of the NSVZ segment (95 km^3 versus <55 km^3 for other centers; Hildreth and Moorbath, 1988); and (ii) it records a distinctive geochemical evolution which has been ascribed to a larger and/or more complex mid- and upper-crustal magma reservoir respect to most other volcanoes from the Andean SVZ (Hildreth and Moorbath, 1988). Respect to the hypothesis discussed in our work, the apparent absence of a compositional shifting towards silicic compositions in this center could be related to specific characteristics of its magmatic reservoir. A large, deep and stably supplied reservoir could remain unaltered by the surficial perturbation that the increased erosion event constitutes in the region.

The simulations discussed in this work represent rather simple magmatic systems but they place tight constraints to the first order parameters that control the magmatic evolution in the context studied. They do not intend to incorporate the innumerous complexities and particularities that individual reservoirs from an arc segment can show and which in turn explain part of the heterogeneities seen in all arcs. These can account for deviations from the predicted compositions, and even differences in the eruptive style, related to characteristics as the depth of emplacement, shape and size of the reservoir, magma supply rate, etc. Moreover, mineral chemistry and petrographic features of samples from the latest Pleistocene silicic stage of the NSVZ account for complex magmatic chamber processes, probably in open systems. Despite all these particularities, the overall processes discussed in this work should develop to a greater or lesser extent throughout the evolution of all cordilleran arc orogenic systems which follow similar tectonomagmatic histories. In this regard, fossil processes of this nature could be the porphyry copper systems which share similar compositions to the ones studied here, have been related to differentiation of deeper magmatic reservoirs, and form under a similar tectonic frame in particular characterized by crustal thickening, uplifting and increased denudation (e.g., Maksaev and Zentilli, 1999; Richards, 2003; Sillitoe, 2010). These might well represent the intrusive equivalent of the high-silica melt segregation and devolatilization processes that occur when the upper crustal magmatic reservoirs are impeded to vent to the surface.

Acknowledgments

This work was supported by the Comisión Nacional de Investigación Científica y Tecnológica (CONICYT, Chile) through projects

ACT-18, PBCT, FONDECYT 1120272 and 1180577, and PAI79160139, and a doctoral grant to the second author IP (PFCHA-CONICYT 21151102). Additional support to coauthor RC from the Freie Universität Berlin and the Alexander von Humboldt Foundation is also acknowledged. We thank the careful reviews of Dr C.R. Stern and an anonymous reviewer.

Appendix A. Supplementary data

Supplementary data to this article can be found online at https://doi.org/10.1016/j.lithos.2019.105242.

References

Aravena, A., Gutiérrez, F.J., Parada, M.A., Payacán, I., Bachman, O., Poblete, F., 2017. Compositional zonation of the shallow La Gloria pluton (Central Chile) by late-stage extraction/redistribution of residual melts by channelization: numerical modeling. Lithos 284–285, 578–587.

Bachmann, O., Bergantz, G.W., 2003. Rejuvenation of the Fish Canyon magma body: a window into the evolution of large-volume silicic magma systems. Geology 31, 789–792.

Bachmann, O., Bergantz, G.W., 2004. On the origin of crystal-poor rhyolites: extracted from batholithic crystal mushes. J. Petrol. 45, 1565–1582.

Baker, S.E., Gosse, J.C., McDonald, E.V., Evenson, E.B., Martínez, O., 2009. Quaternary history of the piedmont reach of Río Diamante, Argentina. J. South Am. Earth Sci. 28, 54–73.

Cahill, T., Isacks, B.L., 1992. Seismicity and shape of the subducted Nazca plate. J. Geophys. Res. 97, 503–529.

Charrier, R., 1981. Geologie chilenischen Hauptkordillere zwischen 34° und 34°30' südlicher Brerite und ihre tektonische, magmatische und peläogeographische Entwicklung. Berliner Geowissenschaftliche Abhandlungen A36.

Charrier, R., Baeza, O., Elgueta, S., Flynn, J.J., Gana, P., Kay, S.M., Muñoz, N., Wyss, A.R., Zurita, E., 2002. Evidence for Cenozoic extensional basin development and tectonic inversion south of the flat-slab segment, southern Central Andes, Chile (33°-36°S.L.). J. South Am. Earth Sci. 15, 117–139.

DeCelles, P., Ducea, M., Kapp, P., Zandt, G., 2009. Cyclicity in Cordilleran orogenic systems. Nat. Geosci. 2, 251–257.

DeMets, C., Gordon, R.G., Argus, D.F., Stein, S., 1990. Current plate motions. Geophys. J. Int. 101, 425–478.

Ducea, M., Barton, M.D., 2007. Igniting flare-up events in Cordilleran arcs. Geology 35, 1047–1050.

Dufek, J., Bachman, O., 2010. Quantum magmatism: magmatic compositional gaps generated by melt-crystal dynamics. Geology 38, 687–690.

Farías, M., Charrier, R., Carretier, S., Martinod, J., Fock, A., Campbell, D., Cáceres, J., Comte, D., 2008. Late Miocene high and rapid surface uplift and its erosional response in the Andes of central Chile (33°-35°S). Tectonics 27, TC1005.

Farías, M., Comte, D., Charrier, R., Martinod, J., Tassara, A., Fock, A., 2010. Crustal-scale structural architecture of the central Chile Andes based on 3D seismic tomography, seismicity, and surface geology: implications for mountain building in subduction zones. Tectonics 29, TC3006.

Futa, K., Stern, C.R., 1988. Sr and Nd isotopic and trace element compositions of Quaternary volcanic centers of the southern Andes. Earth Planet. Sci. Lett. 88, 253–262.

Ghiorso, M.S., Gualda, G.A.R., 2015. An H_2O-CO_2 mixed fluid saturation model compatible with rhyolite-MELTS. Contrib. Mineral. Petrol. 169, 53.

Giambiagi, L.B., Ramos, V.A., 2002. Structural evolution of the Andes in a transitional zone between flat and normal subduction (33°30-33°45'S), Argentina and Chile. J. South Am. Earth Sci. 15, 101–116.

Godoy, E., 1998. Intrusivos sintectónicos entre los ríos Aconcagua y Cachapoal, Andes de Chile central. In: X Congreso Latinoamericano de Geología and VI Congreso Nacional de Geología Económica, pp. 149–154. Buenos Aires, Extended Abstracts.

Godoy, E., Hildreth, W., 2001. Cerro Amarillo rhyolites, advanced AFC in the northern SVZ, Chile. In: III South American Symposium on Isotope Geology Pucón, Proceedings, pp. 21–24.

González-Ferrán, O., 1995. Volcanes de Chile. Instituto Geográfico Militar, Santiago, p. 635.

Gualda, G.A.R., Ghiorso, M.S., Lemons, R.V., Carley, T.L., 2012. Rhyolite-MELTS: a modified calibration of MELTS optimized for silica-rich, fluid-bearing magmatic systems. J. Petrol. 53, 875–890.

Guerstein, P.G., 1993. Origen y significado geológico de la Asociación Piroclástica Pumícea. Pleistoceno de la Provincia de Mendoza entre los 33°30' y 34°40'L.S.. Ph.D. Thesis Facultad de Ciencias Naturales y Museo, Universidad Nacional de La Plata, La Plata, p. 270.

Harrington, R., 1989. The Diamante caldera and Maipo caldera complex in the southern Andes of Argentina and Chile (34°10'S). Rev. Asoc. Geol. Argent. 19, 186–193.

Hickey-Vargas, R., Frey, F.A., Gerlach, D.C., 1986. Multiple source for basaltic arc rocks from the Southern Volcanic Zone of the Andes (34°-41°S): trace element and isotopic evidence for contributions from subducted crust, mantle, and continental crust. J. Geophys. Res. 91, 5963–5983.

Hildreth, W., Moorbath, S., 1988. Crustal contributions to arc magmatism in the Andes of central Chile. Contrib. Mineral. Petrol. 98, 455–489.

Holm, P.M., Søager, N., Dyhr, C.T., Nielsen, M.R., 2014. Enrichments of the mantle sources beneath the Southern Volcanic Zone (Andes) by fluids and melts derived from abraded upper continental crust. Contrib. Mineral. Petrol. 167, 1004.

Irvine, T.N., Baragar, W.R.A., 1971. A guide to the chemical classification of the common volcanic rocks. Can. J. Earth Sci. 8, 523–548.

Jacobsen, S.B., Wasserburg, G.J., 1980. Sm–Nd isotopic evolution of chondrites. Earth Planet. Sci. Lett. 50, 139–155.

Kay, R.W., Kay, S.M., 1993. Delamination and delamination magmatism. Tectonophysics 219, 177–189.

Kay, S.M., Mpodozis, C., Coira, B., 1999. Neogene magmatism, tectonism and mineral deposits of the Central Andes (22°-33°S latitude). In: Skiner, B.J. (Ed.), Geology and Ore Deposits of the Central Andes, vol. 7. Society of Economic Geologists Special Publication, pp. 27–59.

Kay, S.M., Godoy, E., Kurtz, A., 2005. Episodic arc migration, crustal thickening, subduction erosion, and magmatism in the south-central Andes. Geol. Soc. Am. Bull. 117, 67–88.

Lagos, J.M., 2003. Ignimbrita Pudahuel: Caracterización geológica-geotécnica orientada a su respuesta sísmica. Geologist Professional Degree Thesis, Departamento de Geología, Universidad de Chile, Santiago, p. 153.

Lara, L.E., Wall, R., Stockli, D., 2008. La ignimbrita pudahuel (asociación piroclástica pumícea) y la Caldera Diamante (33°S): nuevas edades U-Th-He. In: XVII Congreso Geológico Argentino, Jujui, Proceedings, p. 1365.

Leake, B.E.W., Alan, R., Arps, C.E.S., Birch, W.D., Gilbert, M.C., Grice, J.D., Hawthorne, Ec, Kato, A., Kisch, H.J., Krivovichev, V.G., Linthout, K., Laird, J., Mandarino, J., Maresch, W.V., Nickel, E.H., Rock, N.M.S., Schumacher, J.C., Smith, D.C., Stephenson, N.C.N., Ungaretti, L., Whittaker, E.J.W., Youzhi, G., 1997. Nomenclature of amphiboles; report of the subcommittee on amphiboles of the International Mineralogical Association. Commiss. New Miner. Miner. Name. Europ. J. Mineral. 9, 623–651.

López-Escobar, L., Moreno, H., Tagiri, M., Notsu, K., Onuma, N., 1985. Geochemistry and petrology of lavas from san José volcano, southern Andes. Geochem. J. 19, 209–222.

Maksaev, V., Zentilli, M., 1999. Fission track thermochronology of the Domeyko Cordillera, Northern Chile: implications for Andean tectonics and porphyry copper metallogenesis. Explor. Min. Geol. Spec. Issue Latin Am. Miner. Deposit. 8, 65–89.

Mercer, J.H., 1976. Glacial history of southernmost south America. Quat. Res. 6, 125–166.

Muñoz, M., Farías, M., Charrier, R., Fanning, C.M., Polvé, M., Deckart, K., 2013. Isotopic shifts in the Cenozoic Andean arc of central Chile: records of an evolving basement throughout cordilleran arc mountain building. Geology 41, 931–934.

Nyström, J.O., Vergara, M., Morata, D., Levi, B., 2003. Tertiary volcanism in central Chile (33°15'-33°45'S): a case of andean magmatism. Geol. Soc. Am. Bull. 115, 1523–1537.

Ormeño, A., 2007. Geomorfología dinámica del río Maipo en la zona cordillerana de Chile Central e implicancias neotectónicas. Geologist Professional Degree Thesis, Departamento de Geología, Universidad de Chile, Santiago, p. 147.

Pardo, M., Comte, D., Monfret, T., 2002. Seismotectonic and stress distribution in the central Chile subduction zone. J. South Am. Earth Sci. 15, 11–12.

Pineda, C., 2015. Geocronología U/Pb en circones de la ignimbrita Pudahuel. Departamento de Geología, Universidad de Chile, Santiago, p. 105. Geologist Professional Degree Thesis.

Polanski, J., 1962. Estratigrafía neotectónica y geomorfología del Pleistoceno pedemontano entre los ríos Diamante y Mendoza. Revista de la Asociación Geológica Argentina, 27, pp. 127–149.

Rabassa, J., Clapperton, C.M., 1990. Quaternary glaciations of the southern Andes. Quat. Sci. Rev. 9, 153–174.

Rabassa, J., Evenson, E.B., 1996. Reinterpretación de la estratigrafía glaciaria de la región de San Carlos de Bariloche. In: XIII Congreso Geológico Argentino, Buenos Aires, Proceedings, p. 327.

Rabassa, J., Coronato, A.M., Salemme, M., 2005. Chronology of the Late Cenozoic Patagonian glaciations and their correlation with biostratigraphic units of the Pampean region (Argentina). J. South Am. Earth Sci. 20, 81–103.

Ramos, V.A., Alvarez, P.P., Aguirre, M.B., Godoy, E., 1997. La Cordillera Principal a a latitud del paso Nieves Negras (33°50'S Chile - Argentina). In: VII Congreso Geológico Chileno, Antofagasta, Proceedings, pp. 1704–1708.

Richards, J.P., 2003. Tectono-magmatic precursors for porphyry Cu-(Mo-Au) deposit formation. Econ. Geol. 98, 1515–1533.

Ridolfi, F., Renzulli, A., 2012. Calcic amphiboles in calc-alkaline and alkaline magmas: thermobarometric and chemometric empirical equations valid up to 1,130°C and 2.2 GPa. Contrib. Mineral. Petrol. 163, 877–895.

Schneider, A., Charrier, R., Harrington, R., 1988. Recent Acid Volcanism and Associated Alteration along the High Crest of the Andes between Latitude 33°30'-34°30', Revista Comunicaciones. Departamento de Geología, Universidad de Chile, Santiago, p. 279.

Schnurr, W.B.W., Trumbull, R.B., Clavero, J., Hahne, K., Gardeweg, M., 2007. Twenty-five million years of silicic volcanism in the southern central volcanic zone of the Andes: geochemistry and magma genesis of ignimbrites from 25 to 27°S, 67 to 72°W. J. Volcanol. Geotherm. Res. 166, 17–46.

Sillitoe, R.H., 2010. Porphyry copper systems. Econ. Geol. 105, 3–41.

Sisson, T.W., Bacon, C.R., 1999. Gas-driven filter pressing in magmas. Geology 27, 613–616.

Sruoga, P., Llambías, E.J., Fauqué, L., Schonwandt, D., Repol, D.G., 2005. Volcanological and geochemical evolution of the Diamante caldera-Maipo volcano

complex in the southern Andes of Argentina (34°10'S). J. South Am. Earth Sci. 19, 399–414.
Sruoga, P., Etcheverría, M.P., Feineman, M., Rosas, M., Burkert, C., Ibañes, O., 2012. Complejo Caldera Dimanate-Volcán Maipo (34°10'S, 69°50'O): evolución volcanológica y geoquímica e implicancias en su peligrosidad. Rev. Asoc. Geol. Argent. 69, 508–530.
Stern, C.R., 1989. Pliocene to present migration of the volcanic front, andean southern volcanic zone. Rev. Geol. Chile 16, 145–162.
Stern, C.R., 1991. Role of subduction erosion in the generation of Andean magmas. Geology 19, 78–81.
Stern, C.R., Skewes, A., 1995. Miocene to present magmatic evolution at the northern end of the Andean Southern Volcanic Zone. Andean Geol. 22, 261–272.
Stern, C.R., Amini, H., Charrier, R., Godoy, E., Hervé, F., Varela, J., 1984a. Petrochemistry and age of rhyolitic pyroclastic flows which occur along the drainage valleys of the río Maipo and río Cachapoal (Chile) and the río Yaucha and río Papagayos. Andean Geol. 23, 39–52.
Stern, C.R., Futa, K., Muehlenbachs, K., 1984b. Sr, Nd, Pb and O isotope composition of Late Cenozoic volcanics, northernmost SVZ (33-34ºS). In: Harmon, R.S., Barreiro, B.A. (Eds.), Andean Magmatism: Chemical and Isotopic Constraints. Shiva Press, London, pp. 96–106.
Stern, C.R., Moreno, H., López-Escobar, L., Clavero, J.E., Lara, L.E., Naranjo, J.A., Parada, M.A., Skewes, M.A., 2007. Chilean volcanoes. In: Moreno, T., Gibbons, W. (Eds.), The Geology of Chile. The Geological Society, London, pp. 147–178.
Tassara, A., Götze, H.-J., Schmidt, S.T., Hackney, R., 2006. Three-dimensional density model of the Nazca plate and the Andean continental margin. J. Geophys. Res. 111. B09404.
Thiele, R., 1980. Hoja Santiago, Carta Geológica de Chile No. 39. Instituto de Investigaciones Geológicas, Santiago, 21, 21 map p.
Troncoso, C., 2012. Estudio estratigráfico y de volcanología física de la ignimbrita Pudahuel. Geologist Professional Degree Thesis, Departamento de Geología, Universidad de Chile, Santiago, p. 84.
Wall, R., Lara, L.E., Pérez de Arce, C., 2001. Upper pliocene-lower Pleistocene $^{40}Ar/^{39}Ar$ ages of pudahuel ignimbrite (Diamante-Maipo volcanic complex), chentral Chile (33.5°S). In: 3° South American Symposium on Isotope Geology (SSAGI), Pucón, Digital Abstracts. S4-458.
Watt, S., Pyle, D., Tamsin, M., 2013. The volcanic response to deglaciation: evidence from glaciated arcs and a reassessment of global eruption records. Earth Sci. Rev. 122, 77–102.